

1 **Mass changes of Southern and Northern Inylchek Glacier,**  
2 **Central Tian Shan, Kyrgyzstan during ~1975 and 2007**  
3 **derived from remote sensing data**

4  
5 **Donghui Shangguan<sup>1, 2</sup>, Tobias Bolch<sup>2,3</sup>, Yongjian Ding<sup>1</sup>, Melanie Kröhnert<sup>3</sup>,**  
6 **Tino Pieczonka<sup>3</sup>, Hans-Ulrich Wetzel<sup>4</sup>, Shiyin Liu<sup>1</sup>**

7 [1]{State Key Laboratory of Cryospheric Science, Cold & Arid Regions Environmental &  
8 Engineering Research Institute, Chinese Academy of Sciences, Lanzhou 730000, P.R. China}

9 [2]{Department of Geography, University of Zurich, 8057 Zurich, Switzerland}

10 [3]{Institute for Cartography, Technische Universität Dresden, 01069 Dresden, Germany}

11 [4]{GFZ German Research Centre for Geosciences, Potsdam, Germany}

12  
13 Correspondence to: Donghui SHANGGUAN ([dhguan@lzb.ac.cn](mailto:dhguan@lzb.ac.cn))

14  
15  
16 **Abstract**

17 Glacier melt is an essential wellspring of freshwater for the arid regions surrounding the Tian  
18 Shan. However, the knowledge about glacier volume and mass changes over the last decades  
19 is limited. In the present study, glacier area, glacier dynamics, and mass changes are  
20 investigated for the period ~1975 - 2007 for the Southern Inylchek Glacier (SIG) and the  
21 Northern Inylchek Glacier (NIG), the largest glacier in Central Tian Shan separated by the  
22 regularly draining Lake Merzbacher. The area of NIG increased by  $2.0 \pm 0.1 \text{ km}^2$  (~1.3%) for  
23 the period ~1975 - 2007. In contrast, SIG has shrunk continuously in all investigated periods  
24 since ~1975. Velocities of SIG in central part of ablation region reached ~100 - 120 m/a in  
25 2002/2003 which was slightly higher than the average velocity in 2010/2011 with the main  
26 flow direction towards Lake Merzbacher. The measured velocities at the distal part of the  
27 terminus downstream of Lake Merzbacher were below the uncertainty, indicating very low  
28 flow with even stagnant parts. Geodetic glacier mass balances have been calculated using

29 multi-temporal digital elevation models from KH-9 Hexagon (1974 and 1976), SRTM3  
30 (1999), ALOS PRISM (2006), and SPOT-5 HRG (2007). In general, a continuous mass loss  
31 for both SIG and NIG, could be observed between ~1975 and 2007. For SIG a mass loss of  
32  $0.43 \pm 0.10$  m w.e.  $a^{-1}$  and for NIG a loss of  $0.25 \pm 0.10$  m w.e.  $a^{-1}$  were observed for the  
33 period ~1975 - 1999. For the period 1999 – 2007, the highest mass loss of  $0.57 \pm 0.46$  m w.e.  
34  $a^{-1}$  was found for NIG, whilst SIG showed likely a moderate mass loss of  $0.28 \pm 0.46$  m w.e.  
35  $a^{-1}$ . Both glaciers slightly retreated during this period. Between ~1975 and 1999, we identified  
36 a thickening at the front of NIG with a maximum surface elevation increase of about  $\sim 6$  m  $a^{-1}$   
37 as a consequence of a surge event. In contrast significant thinning ( $>0.5$  m  $a^{-1}$ ) and  
38 comparatively high velocities close to the dam of Lake Merzbacher were observed for SIG,  
39 indicating that Lake Merzbacher enhances glacier mass loss.

40

## 41 **1 Introduction**

42 Meltwater from snow and ice is an important freshwater resource for the arid regions  
43 surrounding the Tian Shan (Sorg et al., 2012). This is especially true for the Tarim Basin in  
44 Xinjiang/Northwest China whose main artery, the Tarim River, is considerably nourished by  
45 glacial melt (Aizen et al., 2007; Sorg et al., 2012). The transboundary Asku River (named  
46 Sary-Djaz in Kryrgyzstan), originating in the Kyrgyz part of the Central Tian Shan and the  
47 main tributary of the Tarim River, contributes about 40% to the overall run-off of the Tarim  
48 River (Mao et al., 2004). The runoff of Aksu River has increased during the last decades (Li  
49 et al., 2008; Liu et al., 2006; Piao et al., 2012). Shen et al. (2009) estimated that 13% of the  
50 annual runoff during 1957 - 2006 in the Aksu River was due to the glaciers imbalance while  
51 Pieczonka and Bolch (2014) estimated an even higher value of  $\sim 20\%$  for the period ~1975 -  
52 2000. Reported shrinkage rates varied up to  $\sim 3.7\%$  for the entire Sary-Djaz Basin during 1990  
53 - 2010 (Osmonov et al., 2013) and  $\sim 8.7\%$  for the neighbouring Ak-Shirak Range during 1977  
54 - 2003 (Aizen et al., 2006). Hence, the runoff increase of Aksu River is at least partly due to  
55 increased glacier melt. Changes of mass balance can be directly linked to climate change and  
56 runoff. Glacier mass balance, however, is traditionally measured in-situ. As this work is  
57 laborious and most of the glaciers are located in remote and hardly accessible terrain,  
58 measurements can only be conducted point wise for few glaciers. Several studies have shown  
59 that remote-sensing derived geodetic mass balance estimates are suitable to extend in-situ  
60 measurements in space and time (e.g. Berthier et al., 2010, Bolch et al., 2011, Gardelle et al.,

61 2013; Paul and Haeberli, 2008), and it's even used to calibrate time series of in-situ  
62 glaciological records (e.g. Zemp et al., 2013).

63 Glaciers in Central Tian Shan experienced significant mass loss over the last decades. Aizen  
64 et al. (2006) determined a thinning rate of  $0.69 \pm 0.37 \text{ m a}^{-1}$  (or  $0.59 \pm 0.31 \text{ m w.e. a}^{-1}$  mass  
65 loss, using a density of  $850 \text{ kg m}^{-3}$  to convert volume to mass changes) for the Ak-Shyrak  
66 Massif, the second largest glacierized massif in the Central Tian Shan, while Pieczonka et al.  
67 (2013) found a mass loss of  $0.42 \pm 0.23 \text{ m w.e. a}^{-1}$  using 1976 KH-9 data and the SRTM3  
68 DEM for several partially debris-covered glaciers in south of Peak Pobeda/Tomür Feng (Peak  
69 Pobeda in Russian/ Tomür Feng in Chinese, it is also named after Jengish Chogsu in Kyrgyz)  
70 with a decreasing trend in the recent period (1999 - 2009).

71 SIG, the largest glacier in the Central Tian Shan, is characterized by a layer of debris altering  
72 both rates and spatial patterns of melting. SIG was investigated by field based method  
73 (ablation measurements [Hagg et al., 2008]) and by remote sensing (velocity measurements  
74 [Li et al. 2013]). However, there is still a lack of volume and mass change investigations. In  
75 the present study we used stereo 1974/1976 KH-9 Hexagon (for ease of understanding, we  
76 unified use ~1975 KH-9), 2006 ALOS PRISM, and 2008 SPOT-5 High Resolution  
77 Geometrical (HRG) data and the 2000 SRTM3 DEM to assess the mass change of SIG and  
78 NIG. In addition, we investigated area changes and the glacier dynamics using Landsat  
79 TM/ETM+ and Terra ASTER imagery.

80

## 81 **2 Study region**

82

83 Inylchek Glacier is located in the Kumarik Catchment, the headwater of the Aksu-Tarim  
84 River Catchment between peak Pobeda / Tomür Feng (7,439 m a.s.l., the highest peaks of the  
85 Tian Shan) and Khan Tengri (6,995 m a.s.l.) (Fig. 1). The glacier consists of two branches:  
86 the Southern and Northern Inylchek Glacier (SIG and NIG) which formerly had a joined  
87 tongue; however, glacier recession led to a separation (Lifton et al., 2014; Kotlyakov et al.,  
88 1997). The space between the two tongues was filled by Merzbacher Lake as the tongue from  
89 the SIG formed an ice-barrier which dammed the meltwater (Glazirin, 2010; Häusler et al.,  
90 2011). SIG stretches about 60.5 km in East - West direction with an area of approximately  
91  $500 \text{ km}^2$ . NIG and SIG together account for ~32% of the total glacier area of the Sary-Djaz

92 river basin (Osmonov et al., 2013). The equilibrium line altitude (ELA) is located at about  
93 4,500 m a.s.l. (Aizen et al., 2007). Existing velocity measurements of SIG show surface  
94 velocities of about  $100 \text{ m a}^{-1}$  for the central part of the ablation region (Li et al., 2013;  
95 Nobakht et al., 2014) where the glacier flow is mainly directed towards Lake Merzbacher  
96 (Mayer et al., 2008; Nobakht et al., 2014).

97 The study region is characterized by a semi-continental climate. Precipitation recorded at  
98 Tian Shan Station (TS) (1960 - 1997) ( $78.2^{\circ}\text{N}$ ,  $41.9^{\circ}\text{E}$ , 3,614 m a.s.l., Fig.1) and Koilu  
99 Station (K) (1960-1990) ( $79.0^{\circ}\text{E}$ ,  $42.2^{\circ}\text{N}$ , 2,800 m a.s.l., Fig.1) was  $279 \text{ mm a}^{-1}$  and  $311 \text{ mm}$   
100  $\text{a}^{-1}$ , respectively (Reyers et al., 2013) with about 75% of precipitation occurring during  
101 summer (May - September). Hence, both SIG and NIG receive a significant amount of the  
102 accumulation during summer as compared to Himalayan Glaciers (Osmonov et al., 2013). No  
103 long-term precipitation measurements exist on the glacier itself. However, a correlation  
104 between annual accumulation measured by stakes at 6,148 m a.s.l. and annual precipitation  
105 was constructed for Tian Shan Station (Aizen et al., 1997). The mean annual temperature at  
106 Tian Shan Station is about  $-7.7^{\circ}\text{C}$  with January being the coldest month ( $-21.8^{\circ}\text{C}$ ) and July  
107 the warmest ( $4.3^{\circ}\text{C}$ ) (Osmonov et al., 2013).

108

### 109 **3 Data and Methods**

#### 110 **3.1 Remote sensing datasets**

111 Declassified KH-9 Hexagon, SPOT-5 HRG, ALOS PRSIM, Terra ASTER, Landsat  
112 TM/ETM+ and SRTM3 data were used to obtain information about surface elevation, surface  
113 velocity and area extent of both SIG and NIG for different periods (Tab. 1).

114 The KH-9 Hexagon mission was part of the US Keyhole reconnaissance satellite program  
115 whose images were declassified in 2002 (Phil, 2013). The employed frame camera system  
116 was used on a total of 12 missions between 1973 and 1980. For the KH-9 missions the same  
117 film as for the KH-4 mission was used. The film resolution is about 85 line pairs/mm. In our  
118 study, we used Hexagon images from mission 1209 flown in November 1974 and mission  
119 1,211 flown in January 1976.

120 For the period around 2000, the unfilled finished Shuttle Radar Topography Mission (SRTM)  
121 data with 3 arc-second resolution (approximately 90-meter) (USGS, 2006) was used. Yang et

122 al. (2011) and Shortridge et al. (2011) reported an absolute vertical accuracy of the SRTM3  
123 DEM of about 10 m. However, the accuracy in mountainous terrain is likely worse  
124 (Gorokhovich et al., 2006; Pieczonka et al., 2011; Surazakov et al., 2006). The original  
125 SRTM3 dataset has some data voids especially at high and steep elevation regions due to  
126 radar shadow and layover effects (Supplementary Figure S1). Thus, parts of the accumulation  
127 regions are not covered by the SRTM3 DEM. These gaps have been filled in the SRTM3  
128 CGIAR version 4 DEM using auxiliary data (Jarvis et al., 2008), but the exact time is only  
129 known for the original data. The void filled SRTM3 DEM was used for the orthorectification  
130 of ASTER images and the calculation of the glacier hypsometry (Supplementary Figure S2).  
131 Due to the acquisition in February 2000 the DEM represents the glacier surface as constituted  
132 at the end of the 1999 ablation period. However, the penetration of the C-band radar waves of  
133 about 1 - 2 m on exposed ice and up to 10 m on dry, cold firn (Gardelle et al., 2012; Rignot et  
134 al., 2001) needs to be taken into account.

135 The SPOT-5 HRG instruments offer across-track stereo images with the viewing angle being  
136 adjustable through  $\pm 27^\circ$  from two different orbits, which are suitable for DEM generation in  
137 high mountain areas (Toutin, 2006). Due to the precise on board measurements of satellite  
138 positions and attitudes of the SPOT-5 orbit, each pixel in a SPOT-5 image can be located on  
139 the ground with an accuracy of  $\pm 25$  m on the 66% confidence level without additional ground  
140 control points (GCPs) (Berthier et al., 2007; Bouillon et al., 2006). Two SPOT-5 HRG images,  
141 acquired on 5 Feb. 2008 with an incidence angle of  $-9.79^\circ$  and  $24.94^\circ$  offering a Base to  
142 Height Ratio (B/H) of about 0.63, were used for DEM generation (Tab. 1). The image  
143 contrast on the glacier of the utilized images is suitable for DEM generation, but several  
144 regions in the SPOT-5 DEM are influenced by cast shadows and were eliminated from the  
145 final DEM (Supplementary Figure S2).

146 ALOS was launched in January 2006, carrying the PRISM optical sensor in a triplet mode, i.e.  
147 in forward, nadir and backward views in along-track direction (Takaku et al., 2004). We used  
148 the nadir and backward images (Tab. 1). The horizontal accuracy of the geometrical model  
149 with Rational Polynomial Coefficients (RPC) (which contains the interior and exterior  
150 information) can achieve an accuracy of better than 6.0 m (or 7.5 m in horizontal direction  
151 and 2.5 m in vertical direction) without any GCPs (Takaku et al., 2004; Uchiyama et al.,  
152 2008). This accuracy can be improved by using additional GCPs.

153 In addition to the above mentioned image we used Landsat TM/ETM+ and Terra ASTER data  
154 to investigate the changes in glacier extent and to observe the glacier flow (Tab. 1).  
155 Unfortunately only SIG was covered by the utilized ASTER scenes.

## 156 **3.2 Glacier boundary**

157 The glacier boundaries were manually delineated from Landsat TM/ETM+, orthorectified  
158 panchromatic SPOT-5 and KH-9 images. Debris cover on the tongue of SIG hampered the  
159 accurate identification of the glacier margin. However, water outlets at the front of SIG and  
160 traces left after the river flow around the tongue are visible in the images. We identified the  
161 lines of the traces surrounding the debris covered ice as the glacier terminus boundary (Fig.  
162 2a). For the NIG terminus boundary the delineation between the water and debris was used as  
163 the terminus boundary of ice (Fig. 2b). Furthermore, the hillshade based on the SRTM3 DEM  
164 provided additional information to detect the glacier boundary. The accuracy of the glacier  
165 outlines is strongly influenced by debris cover and different spatial resolutions of the used  
166 satellite datasets (Paul et al., 2013). We estimated the uncertainty using a buffer of 10 m for  
167 the KH-9 images and half a pixel for Landsat TM/ETM+ images in bare ice region and good  
168 snow conditions (cf. Bolch et al., 2010). For the debris-covered parts, a buffer of 2 pixels of  
169 each images was used to evaluate the delineation uncertainty. We assume that the uncertainty  
170 due to image co-registration is captured with the buffer method. Under consideration of the  
171 law of error propagation, the final uncertainty  $\theta_{change}$  was calculated using equation 1.

$$172 \quad \theta_{change} = \sqrt{\theta_{period1}^2 + \theta_{period2}^2} \quad (1)$$

173 Where  $\theta_{period1}, \theta_{period2}$  represent the uncertainties of the glacier outlines in period1 and period2.  
174 The mapping uncertainties vary between 0.3 - 3.7% (Tab. 2).

## 175 **3.3 Flow velocity of SIG**

176 To investigate the dynamic behaviour of the SIG, we measured glacier displacement rates  
177 using multi-temporal optical satellite image covering a time span of about one year. A  
178 frequency based feature tracking (phase correlation) was performed using the EXELIS VIS  
179 ENVI add-on COSI-Corr in order to get the horizontal offset of corresponding image points.  
180 The tracking was performed using the method of phase correlation. For ASTER data a  
181 previous subpixel-coregistration was performed as described in Leprince et al. (2007) using  
182 the gap-filled SRTM3 CGIAR DEM, which was bilinearly resampled to 30 m, as vertical

183 reference. Landsat level 1T data were assumed to be quasi-coregistered because of the same  
184 sets of GCPs and vertical references used for orthorectification. On the basis of an expected  
185 annual average velocity of SIG of up to 90 m/a (observed in 2003/2004 [Mayer et al., 2008])  
186 and the images' resolution, the step size was set to four pixels for ASTER and two pixels for  
187 Landsat. Hence, both displacement maps have a final resolution of 60 m.

188 The relative offsets of the co-registered images show the phase difference of the previously  
189 Fourier transformed input data and can be estimated by the correlation maximum (Leprince et  
190 al., 2007). For the 2010/2011 observation period, offsets in the north-south and east-west -  
191 direction were measured with an accuracy of 1/7 pixel using quasi coregistered Landsat TM  
192 (L1T) data. For the 2002/2003 period, we achieved a precision of 1/4 pixel based on 1/25  
193 pixel-coregistered ASTER (L1A) data. A Signal-to-Noise Ratio (SNR) of 0.9 was selected  
194 and applied to filter obvious outliers. The reliability of the displacement vectors was assessed  
195 by the ratio of the RMSE and the resolution of the respective input data. Errors caused by  
196 clouds, topography and low image contrast have been removed from the matching result. The  
197 final uncertainty has been determined to be 3.5 m/a for 2002/2003 and 4.7 m/a for 2010/2011.

### 198 **3.4 DEM generation and DEM post processing**

199 KH-9, ALOS PRISM and SPOT-5 HRG data were processed by using Leica Photogrammetry  
200 Suite (LPS), vers. 2013 with the reference system UTM WGS84 Zone 44.

201 For the stereo processing of the KH-9 images, we measured 38 GCPs for the DEM covering  
202 the lower part of Inylchek Glacier and 47 GCPs for the stereo pair covering the accumulation  
203 region of Inylchek Glacier with a final RMSE of ~1 m. GCPs coordinates and elevations were  
204 derived from Landsat 7 ETM+ scenes and the SRTM3 DEM. For the processing, the frame  
205 camera model in LPS, was used and the final resolution of the KH-9 DEMs was 25 m.

206 ALOS PRISM and SPOT-5 were processed with four additional GCPs in order to improve the  
207 accuracy of the exterior orientation (Supplementary Table S1). The automatically generated  
208 tie points (TPs) were visually checked in terms of ground objective and topographic features.  
209 In total, 120 TPs were used. The spatial resolution of the ALOS and SPOT-5 DEMs was 10 m.  
210 Differencing of multi-temporal DEMs necessitates a co-registration including the removal of  
211 horizontal and vertical offsets (Pieczonka et al., 2013). We used the analytical method  
212 proposed by Nuth and Kääb (2011) which has been proven to provide robust results and to be  
213 computationally effective (Paul et al. 2014). All DEMs were bilinearly resampled to the same

214 cell size of 30 m. The resolution is a compromise between the possible higher resolution of  
215 KH-9 and SPOT-5 DEMs and the lower resolution of the SRTM DEM. The shift vectors were  
216 calculated based on selected ice free sample regions (Supplementary Figure S3). The resulting  
217 horizontal shifts were in the order of 2 pixels and the z-offsets varied between 1.3 m and  
218 almost 20 m (Supplementary Table S2).

### 219 **3.5 Radar Penetration**

220 Radar penetration for the SRTM C-band in ice, firn and snow needs to be considered  
221 (Gardelle et al., 2012; Kääb et al., 2012; Mätzler and Wiesmann, 1999). A Landsat ETM+  
222 (Level 1) scene from 18 February, which is within the time of the SRTM mission (11 - 20  
223 February 2000) revealed that SIG and NIG were covered by snow. We used available ICESat  
224 GLA14 footprints to compare with SRTM3 elevation data in order to assess the penetration  
225 depth as described by Kääb et al. (2012). Six out of nine ICESat tracks covering both SIG and  
226 NIG from 2003 to 2004 were selected. We classified those footprints into glacier free terrain,  
227 debris-covered regions (region a and region b), bare ice and accumulation regions  
228 (Supplementary Figure S4). Fortunately, there was an excellent track over 4,300 m a.s.l.. We  
229 eliminated the differences of the elevation change between 2000 and 2003/2004 by using the  
230 elevation change rate between the footprints acquired in 2003 and 2004. The results show a  
231 mean penetration depth of  $-0.1 \pm 3.2$  m for the glacier free terrain,  $1.3 \pm 2.9$  m for the  
232 debris-covered region a,  $-3.6 \pm 4.5$  m for the debris-covered region b (3,500 - 3,600 m a.s.l.)  
233 where some parts are bare ice,  $-4.3 \pm 2.3$  m for bare ice parts in altitudes from 4,000 to 4,300  
234 m a.s.l. and  $-6.8 \pm 2.1$  m for the bare ice parts in altitudes from 4,300 to 5,100 m a.s.l. There  
235 was no data higher than 5,100 m a.s.l.. Furthermore, we compared the SRTM C-band and  
236 SRTM X-band DEMs to estimate the radar penetration based on ICESat footprints (cf.  
237 Gardelle et al., 2012) though 6 - 16 m penetration depth was reported at 10.7 GHz (SRTM  
238 X-band had 10GHz) (Surdyk, 2002). Both DEMs were resampled to 30 m resolution. The  
239 result show that the mean elevation difference within 100 m altitude zones varies between 1.7  
240 m in the lower debris-free ablation area and about 2.1- 4.2 m for altitude within 4,000 - 5,100  
241 m a.s.l. the penetration depth of both lower debris-free ablation region and altitude with 4,000  
242 - 5,100 m a.s.l. was 2.2 - 2.6 m lower as the depth revealed by comparing ICESat GLA to  
243 SRTM3 data. The maximum elevation difference was about 9 m between SRTM C-band and  
244 SRTM X-band DEMs (Supplementary Figure S5), which disagrees with the estimated



245 penetration (9 m at 4,500 m a.s.l.) in Akshirak massif by using a linear method (cf.  
246 Surazakov et al., 2006). The uncertainty of the radar penetration (*erp*) was estimated by the  
247 Standard Deviation (STD) to be 1.9 m. Consequently, the penetration depth was evaluated by  
248 using sum of the difference between SRTM C-band and SRTM X-band DEMs and 2.6 m.  
249 Subsequently, averaged penetration depth in each altitude zone was used to correct elevation  
250 differences.

### 251 3.6 Glacier elevation change and mass balance

252 The elevation change was calculated based on the area-averaged value per 100 m elevation  
253 zone from DEM differencing (cf. Gardner et al., 2013; Xu et al., 2013; Formula 2,  
254 Supplementary Figure S2). After filtering outliers caused by low image contrast (e.g by cast  
255 shadows) for optical data, radar shadow and layover for microwave data in each zone, the  
256 mean volume of each zone was used to calculate the elevation change (Formula 2).

$$257 \quad \Delta h_{gl} = \frac{\sum_{i=1}^n \Delta h_i * s_i}{s_{all \ zones}} \quad (2)$$

258 where  $i$  is the number of zones,  $\Delta h_i$  is the mean glacier elevation change in the respective zone  
259 after radar penetration correction,  $s_i$  is the area of each zone,  $n$  is the total number of zones,  
260 and  $s_{all \ zones}$  is the total area of all zones. The distal part of the tongue of SIG, which is not  
261 covered by the SPOT-5 DEM (Fig. 1), was filled with the ALOS DEM. In order to account  
262 for the different times of image acquisition of ALOS PRISM and SPOT-5 we used the  
263 elevation change per year for filling the gaps of SPOT-5 DEM. A density of  $850 \pm 60 \text{ kg m}^{-3}$   
264 was used to convert the volume to actual mass change (cf. Huss, 2013).

265 The accuracies of the final DEM differences were evaluated with regard to the vertical offset  
266 over ice-free terrain which is supposed to be stable. Outlier values were identified by  $3\sigma$  and  
267 excluded from further processing (cf. Gardelle et al., 2013; Gardner et al., 2013). Due to the  
268 glacier surge in late 1996, outliers of NIG for the period ~1975 - 1999 and ~1975 - 2007 were  
269 defined and excluded as follows: all values larger than the sum of the maximum elevation  
270 difference (which is larger than  $3\sigma$ ) in the surging region, standard deviation and mean of the  
271 elevation difference. After outlier cleaning several obvious errors could still be detected in the  
272 accumulation regions. According to the annual snow-firn layer (the thickness was less than  
273 275 mm/year) at 6,148 m a.s.l. on SIG from 1969 to 1989 (Aizen et al., 1997), the maximum  
274 accumulation can be inferred to be less than 9.1 m (275 mm/year \* 33 years) for the period

275 ~1975 - 2007. The maximum seasonal snow depth in February 2000 was estimated to be 9.0  
 276 m by comparing SRTM C-band and SRTM X-band (cf. section 3.5). Hence, we considered a  
 277 threshold of 20 m (including 2.6 m underestimated) as the maximum accumulation for  
 278 elevations above 4,000 m a.s.l.. In order to analyse the relative uncertainty of the ALOS DEM  
 279 compared to the SPOT-5 DEM we measured a profile with 342 sample points between 3,050  
 280 and 3,350 m a.s.l. on the glacier. The results revealed an uncertainty of 4.5 m with a standard  
 281 deviation of 3.6 m. This uncertainty from ALOS DEM included glacier elevation changes  
 282 between 2006 and 2007.

283 The uncertainty of the differences of the different DEMs was estimated by the normalized  
 284 median absolute deviation (NMAD) (expressed by  $1.4826 * MED(|\tilde{x} - x_i|)$ ,  $x_i$ : elevation  
 285 difference;  $\tilde{x}$ : Median) for the ice free terrain (Supplementary Table S2). Considering the  
 286 radar wave penetration accuracy of 2.3 m, the uncertainty of the DEM differences was  
 287 calculated according to equation 3. The final mass balance uncertainty ( $E$ ) has been calculated  
 288 considering the DEM uncertainty ( $e$ ) where  $t$  is the observation period, ice density ( $\rho_I$ : 850  
 289  $\text{kg/m}^3$ ) the ice density uncertainty ( $\Delta\rho$ : 60  $\text{kg/m}^3$ ), and the water density ( $\rho_w$ : 999.92  $\text{kg/m}^3$ )  
 290 (Equation 4).

291

$$292 \quad e = \sqrt{NMAD^2 + 2.3^2} \quad (3)$$

$$293 \quad E = \frac{e\sqrt{(\Delta\rho)^2 + (\rho_I)^2}}{t * \rho_w} \quad (4)$$

294

## 295 **4 Results**

### 296 **4.1 Glacier flow**

297 We noticed high velocities with an average flow of about ~100 - 120 m/a (between point b  
 298 and point c representing the central ablation region) for SIG towards Lake Merzbacher while  
 299 the remaining part of the debris-covered tongue (between point a and point b, lower ablation  
 300 region/downstream of Lake Merzbacher) has significantly lower velocities with decreasing  
 301 rates and likely stagnant parts at the terminus (Fig. 3). An obvious low flow section (less than  
 302 30 m/a) at point b, upstream of the turn to Lake Merzbacher was observed in both 2002/2003

303 and 2010/2011 (Fig. 3). A significant acceleration was observed from point b to the lake dam.  
304 These results are in agreement with Nobakht et al. (2014).

305 Most tributaries have active flows until the confluence of the glacier with velocities varying  
306 typically between 30 and 60 m/a. The general patterns and velocities in main flow direction  
307 are similar for both investigated periods (2002/2003 and 2010/2011). However, comparing  
308 the velocities of 2002/03 and 2010/11 shows a slight deceleration for the main stream of SIG  
309 (Supplementary Figure S6). Significant deceleration of the surface velocity were found in  
310 region 1 and region 2 (cf. Fig. 3) with high velocities (more than 60 m/a) for the period  
311 2002/2003 and lower velocities (less than 45 m/a) for the period 2010/2011.

## 312 **4.2 Glacier area change**

313 SIG shrank continuously by about  $0.1 \pm 0.1 \text{ km}^2$  ( $0.007 \pm 0.007 \text{ km}^2 \text{ a}^{-1}$ ),  $0.5 \pm 0.1 \text{ km}^2$   
314 ( $0.056 \pm 0.011 \text{ km}^2 \text{ a}^{-1}$ ) and  $0.2 \pm 0.1 \text{ km}^2$  ( $0.025 \pm 0.013 \text{ km}^2 \text{ a}^{-1}$ ) during the periods ~1975  
315 - 1990, 1990 - 1999, and 1999 - 2007. The overall area loss of SIG was  $0.8 \pm 0.1 \text{ km}^2$  ( $0.025$   
316  $\pm 0.003 \text{ km}^2 \text{ a}^{-1}$ ) during ~1975 and 2007, accounting for ~0.2% of its area in ~1975. NIG lost  
317 an area of  $1.2 \pm 0.1 \text{ km}^2$  ( $0.08 \pm 0.007 \text{ km}^2 \text{ a}^{-1}$ ) during the period ~1975 - 1990 followed by  
318 an area increase of  $3.7 \pm 0.1 \text{ km}^2$  ( $0.411 \pm 0.011 \text{ km}^2 \text{ a}^{-1}$ ) during the period 1990 - 1999.  
319 Within this period, the glacier showed a strong advance of about 3.5 km. The glacier shrank  
320 again by  $0.4 \pm 0.1 \text{ km}^2$  ( $0.050 \pm 0.013 \text{ km}^2 \text{ a}^{-1}$ ) in the consecutive period (1999 - 2007).  
321 Overall, the area of the NIG increased by  $2.0 \pm 0.1 \text{ km}^2$  ( $0.063 \pm 0.003 \text{ km}^2 \text{ a}^{-1}$ ) during ~1975  
322 - 2007, accounting for ~1.3% of its area in ~1975 (Fig. 2; Tab. 3). Consequently, the area of  
323 the entire Inylchek Glacier system increased by  $1.3 \pm 0.1 \text{ km}^2$  (~0.2%) between ~1975 and  
324 2007.

## 325 **4.3 Glacier mass change**

326 The mass budget of SIG and NIG was  $-0.43 \pm 0.10 \text{ m w.e. a}^{-1}$  and  $-0.25 \pm 0.10 \text{ m w.e. a}^{-1}$ ,  
327 respectively for the ~1975 - 1999 period, after 1999, a mass budget of  $-0.57 \pm 0.46 \text{ m w.e. a}^{-1}$   
328 was measured for NIG while a mass budget  $-0.28 \pm 0.46 \text{ m w.e. a}^{-1}$  was observed for SIG.  
329 Both SIG and NIG experience a mass loss ( $0.42 \pm 0.11 \text{ m w.e. a}^{-1}$  and  $0.30 \pm 0.11 \text{ m w.e. a}^{-1}$ )  
330 between ~1975 and 2007 (Fig. 4 & Tab. 54). We also noted significant thinning of about 0.5 -  
331 2.0 m  $\text{a}^{-1}$  from ~1975 to 2007 for SIG close to the lake dam (Fig. 4). At this location, high

332 flow velocities were observed (Figure 3), which causes more ice to be transported there (Ng et  
333 al., 2007; Mayer et al., 2008).

334 The elevation differences measured along the main flow line allows more detailed insights  
335 into the characteristics of the glaciers behaviour (Fig. 5). SIG showed a surface lowering  
336 from its terminus to point b for the periods ~1975 - 1999 and 1999 - 2007 (Fig. 5). There are  
337 mean large variation in elevation changes between point a and b below Lake Merzbacher (Fig.  
338 5) where the glacier is heavily debris covered and shows low or even no surface flow (Fig. 3).  
339 A clear surface lowering could be observed upwards the glacier between point b and g for all  
340 investigated periods (Fig. 4 and Fig. 5). We also identified parts with no significant surface  
341 elevation changes at SIG above point c for ~1975 - 1999 (Fig. 4a) until ~37 km from the  
342 terminus (Fig. 5). An apparent elevation increase at a mean rate of  $1 - 2 \text{ m a}^{-1}$  was observed  
343 for the period 1999 - 2007 in region 2 (above point g) of the accumulation region for SIG (Fig.  
344 4b) where decreased velocities were measured for the period 2002 - 2003 and 2011 - 2012  
345 (Fig. 3a). NIG showed a significant thickening with maximum values of  $\sim 6 \text{ m a}^{-1}$  close to the  
346 terminus (point d) for the period ~1975 - 1999 while the glacier rapidly thinned at a rate of  
347  $\sim 4 \text{ m a}^{-1}$  further upwards the glacier tongue (between point e and f; Fig. 5 NIG). Hence, a  
348 large amount of mass was transferred from the accumulation to the ablation region which is a  
349 typical sign for a glacier surge. In contrast, NIG showed a clear thinning throughout the  
350 tongue after 1999.

351 SIG experienced thinning throughout all altitude zones except at elevations between 6,300  
352 and 6,500 a.s.l. for the period ~1975 - 1999. The most obvious thinning was observed at 3,700  
353 - 4,500 and 5,400 - 5,800 m a.s.l.. For the period 1999 - 2007, surface lowering was measured  
354 only below 4,500 m a.s.l. with a mean rate of about  $0.9 \pm 0.5 \text{ m a}^{-1}$ . In contrast clear  
355 thickening with a mean rate of about  $0.2 \pm 0.5 \text{ m a}^{-1}$  was observed between 4,500 - 4,900 m  
356 a.s.l. (Fig. 6; Supplementary Table S3). For the entire investigation period (~1975 - 2007),  
357 the surface elevation of SIG decreased below 6,500 m a.s.l..

358

## 359 **5 Discussion**

360

## 361 **5.1 Uncertainty**

362 Seasonal snow in the accumulation region and debris cover, as also present in our study  
363 region, typically complicated precise glacier mapping (cf. Bolch et al., 2010, Paul et al., 2013).  
364 In order to assess our uncertainty estimate, we compared the results of the buffer method used  
365 with the approach suggested by Pfeffer et al (2014). The results show that the delineation  
366 uncertainty of SIG using their approach with 30 m from Landsat TM was about 9 km<sup>2</sup>, which  
367 is smaller than our results of about 11 km<sup>2</sup>. Hence we think our approach provides a reliable  
368 uncertainty estimate especially as we used a larger buffer of 2 pixels in each images for the  
369 debris-covered parts.

370 One critical issue with all studies using the SRTM3 DEM for geodetic mass balance  
371 calculations is the unknown C-band radar penetration into snow and ice. We estimated the  
372 penetration using ICESat laser altimetry data which is one of the most robust methods in case  
373 field data is not available (Kääb et al., 2012). The uncertainty for our mass balance estimation  
374 is also strongly influences by the penetration correction. The estimated mean SRTM  
375 penetration for both SIG and NIG was  $4.8 \pm 1.9$  m. This is larger than the correction  
376 estimated for the Karakorum (Gardelle et al., 2013) and Hindu Kush (Kääb et al., 2012). The  
377 correction for radar penetration decreases the mass budgets on average by 0.17 m w.e. for the  
378 period ~ 1975 - 1999 and by 0.51 m w.e. for the period 1999 - 2007.

379 One of the further major uncertainties in our study is caused by the lack of information in  
380 several altitudinal zones due to data voids in the accumulation regions (Supplementary Figure  
381 2). Pieczonka et al. (2013) used different suitable assumptions to fill the data voids in  
382 accumulation regions. In this study, the maximum, minimum and mean elevation changes  
383 observed in the accumulation regions were used to fill the voids and to evaluate the impact on  
384 the whole glacier mass balance. We found that the area in those zones were too small (0.5%  
385 above 6,500 m a.s.l. in area) to affect the results significantly. The different assumptions led  
386 to a variation of the mass balance by only  $< 0.02$  m a<sup>-1</sup>. This number was added in to the  
387 uncertainty terms.

## 388 **5.2 Glacier changes**

389 Our study revealed only a slight retreat of SIG during ~1975 and 2007 while a strong advance  
390 for NIG could be identified between 1990 and 2000. Osmonov et al. (2013) reported an

391 average shrinkage of  $3.7 \pm 2.7\%$  from 1990 to 2010 with 10 advancing glaciers in the upper  
392 Aksu Catchment. Our results tend to be in agreement with Osmonov et al. (2013) who,  
393 however, did not analyse SIG and NIG separately and did not report the NIG surge. Glacier  
394 shrinkage in adjacent regions such as in Northern Tian Shan (Bolch, 2007; Aizen et al., 2006),  
395 or eastern/Chinese part of Tian Shan (Ding et al., 2006), was significantly larger.

396 Our observed velocities for SIG ( $\sim 120 \text{ m a}^{-1}$  for the main tongue) are in agreement with  
397 Nobakht et al. (2014) and Neelmeijer et al. (2014) who measured velocities rate of  $0.3 - 0.4 \text{ m}$   
398  $\text{day}^{-1}$  ( $\sim 100 - 150 \text{ m a}^{-1}$ ) based on ASTER and Landsat data, but larger than the  $0.2 \text{ m day}^{-1}$   
399 ( $\sim 75 \text{ m a}^{-1}$ ) noted by Li et al. (2013) based on ALOS PALSAR data. The velocity close to  
400 Lake Merzbacher between 2002 and 2003 ( $75 - 90 \text{ m a}^{-1}$ ) is also in agreement with in-situ  
401 measurements ( $80 - 90 \text{ m a}^{-1}$ , Mayer et al., 2008). Glacier calving could be observed for the  
402 SIG with mean velocities of up to  $0.4 \text{ m day}^{-1}$  between 2009 and 2010 (Nobakht et al., 2014).  
403 Furthermore, the elevation changes were about  $-2.0 - -0.5 \text{ m a}^{-1}$  for the periods  $\sim 1975 - 1999$   
404 and  $1999 - 2007$  near the lake dam. Flow velocities at the central ablation region of SIG  
405 (between point b and point c) were higher than at the tongue below Lake Merzbacher  
406 (between point a and point b, Fig. 3). High velocities transport mass from upstream and offset  
407 the mass loss due to ice melt. Furthermore, the water probably also lubricates the glacier bed  
408 (Quincey et al., 2009; Neelmeijer et al., 2014). Hence, the lake likely causes the high velocity  
409 until the lake margin and enhances glacier mass loss (cf. Mayer et al. 2008).

410 Geodetic mass balance measurements of 12 mainly debris-covered glaciers south of Pik  
411 Pobeda/Tomur Peak close to our study area revealed that most of the glaciers have been  
412 losing mass with rates between  $0.08 \pm 0.15 \text{ m w.e. a}^{-1}$  and  $0.80 \pm 0.15 \text{ m w.e. a}^{-1}$  for the time  
413 period 1976 - 2009 (Pieczonka et al., 2013) and two glaciers gained mass and one glacier  
414 (Qingbingtan Glacier No.74) showed signs of a surge similar to NIG. The mass loss was  
415 lower during the last decade (1999 - 2009) than before 1999 (Pieczonka et al., 2013). This  
416 tendency is in line with our results for SIG where we found on average a clear mass loss  
417 during 1975 - 1999 followed by a decreased mass loss between 1999 and 2007, but it is a little  
418 difference for NIG which showed surge-type behaviour. Existing in-situ mass balance  
419 measurements in the Tian Shan also show clearly negative mass budgets since the beginning  
420 of the measurements in the 1960s (WGMS 2013; Sorg et al. 2012). The mass balance from  
421 Kara Batkak and Tuyuksu glaciers, for instance, was  $-0.77 \text{ m w.e. a}^{-1}$  and  $-0.59 \text{ m w.e. a}^{-1}$   
422 between 1974 and 1990, respectively and the mass balance of Tuyuksu Glacier was  $-0.35 \text{ m}$

423 w.e.  $a^{-1}$  from 1999 to 2007 (Unger-Shayesteh et al., 2013; WGMS, 2013; Cao, 1998). The  
424 tendency of Tuyuksu Glacier mass balance in the recent period is in line with the observed  
425 mass loss for SIG for which we found an average mass loss about  $-0.43 \pm 0.10$  m w.e.  $a^{-1}$   
426 during ~1975 - 1999 followed by mass loss of  $-0.28 \pm 0.46$  m w.e.  $a^{-1}$  during 1999 -2007.  
427 However, the mass balance of the Urumqi Glacier No.1 was  $-0.24$  m w.e. $a^{-1}$  during 1975 -  
428 1999, and  $-0.63$  m w.e.  $a^{-1}$  during 1999 - 2007 (Wang et al., 2012; WGMS, 2013). This  
429 tendency is in line with our results for NIG for which found on average a mass loss ( $-0.25 \pm$   
430  $0.10$  m w.e.  $a^{-1}$ ) during ~1975 - 1999 followed by an accelerating mass loss ( $-0.57 \pm 0.46$  m  
431 w.e.  $a^{-1}$ ) during 1999 -2007 although both glaciers are very different in size and characterisitcs.  
432 Further studies based on ICESat laser altimetry pointed out that, on average, glaciers in the  
433 Tian Shan underwent clear mass loss between 2003 - 2009 ( $-0.58 \pm 0.21$  m w.e.  $a^{-1}$ ) (Gardner  
434 et al., 2013). Furthermore, the elevation change for SIG is more pronounced in lower altitude  
435 than in higher altitudes regions as seen from the two ICESat profiles. Comparison with our  
436 result, it is different in this region.

437 The clear thickening at the tongue of NIG and a lowering in higher altitudes (Fig. 5) together  
438 with the data of area and length change are a clear indicator for a surge event that happened  
439 between 1990 and 1999. The surge event of the NIG probably happened in late 1996 with an  
440 advance of about two kilometres (Maylyudov (1998) cit. in Häusler et al. 2011). Surging  
441 glaciers in the Tian Shan were also reported by Narama et al. (2010), Osmonov et al. (2013),  
442 Pieczonka et al. (2013), Pieczonka and Bolch (2014) and in earlier times by Dolgoushin and  
443 Osipova (1975). However, NIG surging was a non-typical surging event due to the lack of  
444 surge characteristics such as: areas of stretched ogives, erosion scars, transverse crevasses or  
445 breaching structures; Hodkins et al. (2009) described this phenomenon as partial surges. NIG  
446 showed a different behaviour in more or less all altitudes which can be explained by due to its  
447 surge-type. However, compared to elevation changes in the same altitude of SIG for the  
448 period 1999 - 2007, NIG experienced higher thinning between elevation 3,300 - 3,600 m a.s.l.  
449 ( $2.0 \pm 0.5$  m  $a^{-1}$ ) than SIG ( $1.2 \pm 0.5$  m  $a^{-1}$ ). Consequently, the more pronounced thinning at  
450 the tongue in comparison to SIG could be due to the quiescent phase after the surge.

451 Both parts of the ablation regions of SIG and NIG are covered by debris below ~ 3,500 m a.s.l.  
452 The surface of SIG showed considerable thinning rates but also great variability for both  
453 investigated time periods of ~1975 - 1999 and ~1975 - 2007. The surface lowering is higher at  
454 the frontal part of SIG despite thick debris cover. This is in line with several other studies

455 which found significant mass loss despite debris cover (Bolch et al., 2011; Kääb et al., 2012;  
456 Nuimura et al., 2012; Pieczonka et al., 2013). Field based measurements in 2005 of moraine  
457 thickness and ablation rates on the SIG revealed a dependency of ablation upon debris  
458 thickness with ablation rates from 2.8 to 6.7 cm/day with a mean of 4.4 cm/day (Hagg et al.,  
459 2008). The lower velocities and even immobility downstream of Lake Merzbacher indicate  
460 that there was little mass supplied from upstream. Therefore, the significant mass loss in  
461 debris-covered region can be explained by the influence of backwasting at ice cliffs and  
462 melting at supraglacial ponds (Fujita and Sakai, 2009; Han et al., 2010; Juen et al., 2014) but  
463 likely also to be a consequence of little mass gain from the accumulation region due to low  
464 flow velocities or even stagnancy (Benn et al., 2012, Bolch et al., 2012; Quincey et al., 2009;  
465 Schomacker, 2008).

466 Measurements at the Tian Shan Station (3,614 m a.s.l.) located 120 km west of SIG revealed  
467 increasing temperature and decreasing precipitation during the ablation season (May-  
468 September) for the period 1970 - 1996; and a decreasing temperature and slightly decreasing  
469 precipitation was measured in the ablation season for the period of 1997-2009 (Krysanova et  
470 al., 2014; Osmonov et al., 2013; Reyers et al., 2013). This is in disagreement with the  
471 observed climate change in the Tarim Basin where temperature increased after 1985 and  
472 annual precipitation increased after 1980 (Chen et al., 2009; Shi et al., 2006). Hence, the  
473 observed significant glacier mass loss between ~1975 and 1999 is most likely a consequence  
474 of the ablation season warming and precipitation decrease which led to an accelerated melting  
475 and less accumulation. Reduced mass loss of SIG between 1999 and 2007 can likely be  
476 explained by reduced ablation due to decreasing temperature. However, increased mass loss  
477 of NIG between 1999 and 2007 can be explained by high mass loss at the tongue of NIG as a  
478 result of strong advance in the mid 1990s.

479

## 480 **6 Conclusion**

481

482 We investigated glacier velocity, glacier area, surface elevation, and mass changes of  
483 Southern and Northern Inylchek glacier for the ~1975 - 2007 period based on multi-temporal  
484 space-borne datasets such as KH-9 Hexagon, Landsat, and SPOT-5 HRG data. Our results  
485 show that SIG has a velocity of about  $100 \text{ m a}^{-1}$  for large parts upstream of Lake Merzbacher  
486 with a main flow direction towards Lake Merzbacher and clearly lower velocities with likely



487 stagnant parts downstream of the lake. Decreasing velocities at the SIG tongue was found  
488 when comparing surface displacements in 2002/2003 to 2010/2011. In general, the area of the  
489 entire Inylchek Glacier system decreased in the ~1975 - 2007 period. However, NIG was  
490 surging later in 1996 which caused an overall area increase of  $2.0 \pm 0.1 \text{ km}^2$  (~1.3%) between  
491 ~1975 and 2007. The generated DEMs from ~1975 and 2007 were of good quality though  
492 partially missing information in the accumulation regions resulted in higher uncertainties.  
493 The results showed that the mass balance of both SIG and NIG was negative from ~1975 to  
494 2007. However, the amplitude of both glaciers' mass loss is different. For SIG, decreased  
495 mass loss in the recent decade was observed with an overall mass balance of  $0.42 \pm 0.11 \text{ m}$   
496  $\text{w.e. a}^{-1}$  between ~1975 and 2007. For NIG, on the other hand, increased mass loss could be  
497 found since 1999; a mass balance of about  $-0.30 \pm 0.11 \text{ m w.e. a}^{-1}$  was measured for the  
498 entire investigated period. Despite thick debris cover, surface lowering is highest at the distal  
499 part of the tongue of SIG where also low velocities are prevailing. The thinning at the lake  
500 dam was higher with a high flow velocity until the calving front, likely caused by calving into  
501 Lake Merzbacher. Thus, glacier thinning and glacier flow is significantly influenced by the  
502 lake.

503

## 504 **Acknowledgements**

505 This work was supported by the Ministry of Science and Technology of the People's Republic  
506 of China (Grant 2013CBA01808); State Key Laboratory of Cryospheric Sciences (SKLCS-  
507 ZZ-2012-00-02); the National Natural Science Foundation of China (Grant: 41271082 &  
508 41030527); the CAS Strategic Priority Research Program-Climate Change: Carbon Budget  
509 and Relevant Issue (Grant No. XDA05090302), German Research Foundation (Deutsche  
510 Forschungsgemeinschaft, DFG, code BO 3199/2-1) and the German Ministry of Education  
511 and Science (BMBF: Code 01 LL 0918 B). China Scholarship Council supported the research  
512 stay of the first author at University of Zurich. We also thank the groups of Bolot  
513 Moldobekov from Central-Asia Institute for Applied Geosciences (CAIAG) for supporting  
514 our field work in 2010 and 2012. ASTER GDEM and SRTM is a product of METI and  
515 NASA. We thank DLR for free access to SRTM X-band data and USGS for free access to  
516 SRTM C-band and Landsat data.

517

518 Author contributions: The study concept was developed by D.S. and T.B. The digital  
519 elevation models were generated by D.S. and T.P. The glacier surface velocities were  
520 calculated by M. Kröhnert. D.S. performed the data analysis and wrote the draft of the paper.  
521 D.S., T.B. and all other authors were involved in paper writing and the revision process.

522

## 523 **Reference**

524 Aizen, V. B., Aizen, E. M., and Kuzmichonok, V. A.: Glaciers and hydrological changes in  
525 the Tien Shan: simulation and prediction, *Environmental Research Letters*, 2, 10.1088/1748-  
526 9326/2/4/045019, 2007.

527 Aizen, V. B., Aizen, E., Dozier, J., and Melack, J. M.: Glacier regime of the highest Tien  
528 Shan mountain, Pobeda-Khan Tengry Massif, *Journal of Glaciology*, 43, 503-512, 1997.

529 Aizen, V. B., Kuzmichenok, V. A., Surazakov, A. B., and Aizen, E. M.: Glacier changes in  
530 the central and northern Tien Shan during the last 140 years based on surface and remote-  
531 sensing data, *Ann. Glaciol.*, 43, 202-213, 2006.

532 Benn, D. I., Bolch, T., Hands, K., Gulley, J., Luckman, A., Nicholson, L. I., Quincey, D.,  
533 Thompson, S., Toumi, R., and Wiseman, S.: Response of debris-covered glaciers in the  
534 Mount Everest region to recent warming, and implications for outburst flood hazards, *Earth-  
535 Science Reviews*, 114, 156-174, <http://dx.doi.org/10.1016/j.earscirev.2012.03.008>, 2012.

536 Berthier, E., Arnaud, Y., Kumar, R., Ahmad, S., Wagnon, P., and Chevallier, P.: Remote  
537 sensing estimates of glacier mass balances in the Himachal Pradesh (Western Himalaya,  
538 India), *Remote Sensing of Environment*, 108, 327-338, DOI 10.1016/j.rse.2006.11.017, 2007.

539 Berthier, E., Schiefer, E., Clarke, G. K. C., Menounos, B., and Remy, F.: Contribution of  
540 Alaskan glaciers to sea-level rise derived from satellite imagery, *Nature geoscience*, 3, 92-95,  
541 10.1038/NGEO737, 2010.

542 Bolch, T.: Climate change and glacier retreat in northern Tien Shan (Kazakhstan/Kyrgyzstan)  
543 using remote sensing data, *Global and Planetary Change*, 56, 1-12, 2007.

544 Bolch, T., Menounos, B., and Wheate, R.: Landsat-based inventory of glaciers in western  
545 Canada, 1985-2005, *Remote Sensing of Environment*, 114, 127-137, 2010.

546 Bolch, T., Pieczonka, T. and Benn, D. I.: Multi-decadal mass loss of glaciers in the Everest  
547 area (Nepal, Himalaya) derived from stereo imagery, *Cryosphere*, 5, 349–358, 2011.

548 Bolch, T., Kulkarni, A., Kääb, A., Huggel, C., Paul, F., Cogley, J. G., Frey, H., Kargel, J. S.,  
549 Fujita, K., Scheel, M., Bajracharya, S. and Stoffel, M.: The state and fate of Himalayan  
550 glaciers, *Science*, 336, 310–314, 2012.

551 Bouillon, A., Bernard, M., Gigord, P., Orsoni, A., Rudowski, V., and Baudoin, A.: SPOT 5  
552 HRS geometric performances: Using block adjustment as a key issue to improve quality of  
553 DEM generation, *Isprs Journal of Photogrammetry and Remote Sensing*, 60, 134-146,  
554 <http://dx.doi.org/10.1016/j.isprsjprs.2006.03.002>, 2006.

555 Cao, M. S.: Detection of abrupt changes in glacier mass balance in the Tien Shan Mountains,  
556 *Journal of Glaciology*, 44, 352-358, 1998.

557 Chen, Y., Xu, C., Hao, X., Li, W., Chen, Y., Zhu, C., and Ye, Z.: Fifty-year climate change  
558 and its effect on annual runoff in the Tarim River Basin, China, *Quaternary International*, 208,  
559 53-61, <http://dx.doi.org/10.1016/j.quaint.2008.11.011>, 2009.

560 Ding, Y., Liu, S., Li, J., and Shanguan, D.: The retreat of glaciers in response to recent  
561 climate warming in western China, *Annals of Glaciology*, 43, 97-105, 2006.

562 Dolgoushin, L. D., & Osipova, G. B.: Glacier surges and the problem of their forecasting.  
563 Moscow: Proc. Snow and Ice Symposium (13 pp.), 1975.

564 Fujita, K., Sakai, A., Nuimura, T., Yamaguchi, S., and Sharma, R. R.: Recent changes in Imja  
565 Glacial Lake and its damming moraine in the Nepal Himalaya revealed by in situ surveys and  
566 multi-temporal ASTER imagery, *Environmental Research Letters*, 045205, 10.1088/1748-  
567 9326/4/4/045205, 2009.

568 Gardelle, J., Berthier, E., and Arnaud, Y.: Impact of resolution and radar penetration on  
569 glacier elevation changes computed from DEM differencing, *Journal of Glaciology*, 58, 419-  
570 422, 10.3189/2012JoG11J175, 2012.

571 Gardelle, J., Berthier, E., Arnaud, Y., and Kääb, A.: Region-wide glacier mass balances over  
572 the Pamir-Karakoram-Himalaya during 1999-2011, *The Cryosphere*, 7, 1263-1286,  
573 10.5194/tc-7-1263-2013, 2013.

574 Gardner, A. S., Moholdt, G., Cogley, J. G., Wouters, B., Arendt, A. A., Wahr, J., Berthier, E.,  
575 Hock, R., Pfeffer, W. T., Kaser, G., Ligtenberg, S. R. M., Bolch, T., Sharp, M. J., Hagen, J.  
576 O., van den Broeke, M. R., and Paul, F.: A Reconciled Estimate of Glacier Contributions to  
577 Sea Level Rise: 2003 to 2009, *Science*, 340, 852-857, 10.1126/science.1234532, 2013.

578 Glazirin, G. E.: A century of investigations on outbursts of the ice-dammed lake  
579 Merzbacher(central Tien Shan), *Austrian Journal of Earth Sciences*, 103, 171-178, 2010.

580 Gorokhovich, Y., and Voustianiouk, A.: Accuracy assessment of the processed SRTM-based  
581 elevation data by CGIAR using field data from USA and Thailand and its relation to the  
582 terrain characteristics, *Remote Sensing of Environment*, 104, 409-415,  
583 <http://dx.doi.org/10.1016/j.rse.2006.05.012>, 2006.

584 Hagg, W., Mayer, C., Lambrecht, A., and Helm, A.: Sub-debris melt rates on southern  
585 Inylchek Glacier, Central Tian Shan., *Geogr. Ann.*, 90A, 55-63, 2008.

586 Han, H., Wang, J., Wei, J., and Liu, S.: Backwasting rate on debris-covered Koxkar glacier,  
587 Tuomuer Mountain, China, *Journal of Glaciology*, 56, 287-296,  
588 [10.3189/002214310791968430](https://doi.org/10.3189/002214310791968430), 2010.

589 Häusler, H., Scheibz, J., Leber, B., Kopecny, A., Echlter, H., Wetzler, H.-U., and Moldobekov,  
590 B.: Results from the 2009 geoscientific expedition to the Inylchek glacier, Central Tien  
591 Shan(Kyrgyzstan), *Austrian Journal of earth sciences*, 104, 47-57, 2011.

592 Huss, M.: Density assumptions for converting geodetic glacier volume change to mass change,  
593 *The Cryosphere*, 7, 877-887, [10.5194/tc-7-877-2013](https://doi.org/10.5194/tc-7-877-2013), 2013.

594 Jarvis, A., Reuter, H. I., Nelson, A., and Guevara, E.: Hole-filled SRTM for the globe Version  
595 4, available from the CGIAR-CSI SRTM 90m Database (<http://srtm.csi.cgiar.org>), 2008.

596 Juen, M., Mayer, C., Lambrecht, A., Haidong, H., and Shiyin, L.: Impact of varying debris  
597 cover thickness on ablation: a case study for Koxkar glacier in the Tien Shan, *The*  
598 *Cryosphere*, 8, 377-386, [10.5194/tc-8-377-2014](https://doi.org/10.5194/tc-8-377-2014), 2014.

599 Kääb, A., Berthier, E., Nuth, C., Gardelle, J., and Arnaud, Y.: Contrasting patterns of early  
600 twenty-first-century glacier mass change in the Himalayas, *Nature*, 488, 495-498, 2012.

601 Kotlakov, V. M.: *World atlas of snow and ice resources*, Institute of Geography, Russian  
602 Academy of Science, Moscow, 371 pp., 1997.

603 Krysanova, V., Wortmann, M., Bolch, T., Merz, B., Duethmann, D., Walter, J., Huang, S.,  
604 Tong, J., Buda, S., and Kundzewicz, Z. W.: Analysis of current trends in climate parameters,  
605 river discharge and glaciers in the Aksu River basin (Central Asia), *Hydrological Sciences*  
606 *Journal*, [10.1080/02626667.2014.925559](https://doi.org/10.1080/02626667.2014.925559), 2014.

607 Leprince, S., Barbot, S., Ayoub, F., Avouac, J. P.: Automatic and precise orthorectification,  
608 coregistration, and subpixel correlation of satellite images, application to ground deformation  
609 measurements. *IEEE Transactions on Geoscience and Remote Sensing*, 45(6): 1529-1558,  
610 2007.

611 Li Jia, L. Z.-W., Wang Chang-Cheng, Zhu Jian-Jun, and Ding Xiao-Li: Using SAR offset-  
612 tracking approach to estimate surface motion of the South Inylchek Glacier in Tianshan,  
613 *Chinese Journal Geophysics*, 56, 1226-1236, 2013.

614 Li, X., Cheng, G., Jin, H., Kang, E., Che, T., Jin, R., Wu, L., Nan, Z., Wang, J., and Shen, Y.:  
615 Cryospheric change in China, *Global and Planetary Change*, 62, 210-218,  
616 <http://dx.doi.org/10.1016/j.gloplacha.2008.02.001>, 2008.

617 Lifton, N., Beel, C., Hättestrand, C., Kassab, C., Rogozhina, I., Heermance, R., Oskin, M.,  
618 Burbank, D., Blomdin, R., Gribenski, N., Caffee, M., Goehring, B. M., Heyman, J., Ivanov,  
619 M., Li, Y., Li, Y., Petrakov, D., Usubaliev, R., Codilean, A. T., Chen, Y., Harbor, J., and  
620 Stroeven, A. P.: Constraints on the late Quaternary glacial history of the Inylchek and Sary-  
621 Dzaz valleys from in situ cosmogenic  $^{10}\text{Be}$  and  $^{26}\text{Al}$ , eastern Kyrgyz Tian Shan, *Quaternary*  
622 *Science Reviews*, 101, 77-90, <http://dx.doi.org/10.1016/j.quascirev.2014.06.032>, 2014.

623 Liu, S. Y., Ding, Y. J., Shangguan, D. H., Zhang, Y., Li, J., Han, H. D., Wang, J., and Xie, C.  
624 W.: Glacier retreat as a result of climate warming and increased precipitation in the Tarim  
625 river basin, northwest China, *Annals of Glaciology*, Vol 43, 2006, 43, 91-96, 2006.

626 Mao, W.Y., Chen, C., Duan, J.J., Su, H.C., Wang, S.F., Wang, J., Ge F.Y.: Streamflow  
627 regime of four source streams and mainstream of Tarim River, Xinjiang, in 2000, *Journal of*  
628 *Glaciology and Geocryology*, 26(4): 488-495, 2004.

629 Mätzler, C., and Wiesmann, A.: Extension of the Microwave Emission Model of Layered  
630 Snowpacks to Coarse-Grained Snow, *Remote Sensing of Environment*, 70, 317-325,  
631 [http://dx.doi.org/10.1016/S0034-4257\(99\)00047-4](http://dx.doi.org/10.1016/S0034-4257(99)00047-4), 1999.

632 Mayer, C., Hagg, W., Lambrecht, A., Helm, A., Scharrer, K.: Post-drainage ice dam response  
633 at Lake Merzbacher, Inylchek glacier, Kyrgyzstan. *Geografiska Annaler*, 90(1): 87-96, 2008.

634 Narama, C., Käab, A., Duishonakunov, M., and Abdrakhmatov, K.: Spatial variability of  
635 recent glacier area changes in the Tien Shan Mountains, Central Asia, using Corona (~1970),  
636 Landsat (~2000), and ALOS (~2007) satellite data, *Global and Planetary Change*, 71, 42-54,  
637 <http://dx.doi.org/10.1016/j.gloplacha.2009.08.002>, 2010.

638 Neelmeijer, J., Motagh, M., and Wetzel, H.-U.: Estimating Spatial and Temporal Variability  
639 in Surface Kinematics of the Inylchek Glacier, Central Asia, using TerraSAR-X Data,  
640 Remote Sensing, 6, 9239-9259, 2014.

641 Ng, F., Liu, S., Mavlyudov, B., and Wang, Y.: Climateic control on the peak discharge of  
642 glacier outburst floods, Geophys. Res. Lett., 34, 10.1029/2007GL0314, 2007.

643 Nobakht, M., Motagh, M., Wetzel, H.-U., Roessner, S., and Kaufmann, H.: The Inylchek  
644 Glacier in Kyrgyzstan, Central Asia: Insight on Surface Kinematics from Optical Remote  
645 Sensing Imagery, Remote Sensing, 6, 841-856, 2014.

646 Nuimura, T., Fujita, K., Yamaguchi, S., and Sharma, R. R.: Elevation changes of glaciers  
647 revealed by multitemporal digital elevation models calibrated by GPS survey in the Khumbu  
648 region, Nepal Himalaya, 1992-2008, Journal of Glaciology, 58, 648-656,  
649 10.3189/2012JoG11J061, 2012.

650 Nuth, C., and Kääb, A.: Co-registration and bias corrections of satellite elevation data sets for  
651 quantifying glacier thickness change, The Cryosphere, 5, 271-290, 10.5194/tc-5-271-2011,  
652 2011.

653 Osmonov, A., Bolch, T., Xi, C., Kurban, A., and Guo, W.: Glacier characteristics and changes  
654 in the Sary-Jaz River Basin (Central Tien Shan, Kyrgyzstan) – 1990–2010, Remote Sensing  
655 Letters, 4, 725-734, 10.1080/2150704x.2013.789146, 2013.

656 Paul, F., and Haeberli, W.: Spatial variability of glacier elevation changes in the Swiss Alps  
657 obtained from two digital elevation models, Geophysical Research Letters, 35, L21512, Doi  
658 10.1029/2008gl034718, 2008.

659 Paul, F., Barrant, N. E., Berthier, E., Bolch, T., Casey, K., Frey, H., Joshi, S. P., Konovalov,  
660 V., Bris, P. L., Molg, N., NOsenko, G., Nuth, C., Pope, A., Racoviteanu, A., Rastner, P., Raup,  
661 B., and Scharrer, K.: On the accuracy of glacier outlines derived from remote-sensing data,  
662 Ann. Glaciol., 54, 171-182, 10.3189/2013AoG63A296, 2013.

663 Paul, F., Bolch, T., Kääb, A., Nagler, T., Nuth, C., Scharrer, K., Shepherd, A., Strozzi, T.,  
664 Ticconi, F., Bhambri, R., Berthier, E., Bevan, S., Gourmelen, N., Heid, T., Jeong, S., Kunz,  
665 M., Lauknes, T. R., Luckman, A., Merryman, J., Moholdt, G., Muir, A., Neelmeijer, J., Rankl,  
666 M., VanLooy, J., and Van Niel, T.: The glaciers climate change initiative: Methods for  
667 creating glacier area, elevation change and velocity products, Remote Sensing of  
668 Environment, <http://dx.doi.org/10.1016/j.rse.2013.07.043>, 2014.

669 Pfeffer, W. T., Arendt, A. A., Bliss, A., Bolch, T., COgley, J. G., Gardner, A. S., Hagen, J.-O.,  
670 Hock, R., Kaser, G., Kienholz, C., Miles, E. S., Moholdt, G., Molg, N., Paul, F., Radic, V.,  
671 Rastner, P., Raup, B. H., Rich, J., Sharp, M. J., and Consortium, T. R.: The Randolph Glacier  
672 Inventory: a globally complete inventory of glaciers, *Journal of Glaciology*, 60, 537-552,  
673 2014.

674 Phil Pressel: Meeting the Challenge: The Hexagon KH-9 Reconnaissance Satellite. American  
675 Institute of Aeronautics and Astronautics, Inc., Reston, Virginia, 2013.

676 Piao, S., Ciais, P., Huang, Y., Shen, Z., Peng, S., Li, J., Zhou, L., Liu, H., Ma, Y., Ding, Y.,  
677 Friedlingstein, P., Liu, C., Tan, K., Yu, Y., Zhang, T., and Fang, J.: The impacts of climate  
678 change on water resources and agriculture in China, *nature*, 467, 10.1038/nature09364, 2010.

679 Pieczonka, T., Bolch, T., and Buchroithner, M.: Generation and evaluation of multitemporal  
680 digital terrain models of the Mt. Everest area from different optical sensors, *Isprs Journal of*  
681 *Photogrammetry and Remote Sensing*, 66, 927-940,  
682 <http://dx.doi.org/10.1016/j.isprsjprs.2011.07.003>, 2011.

683 Pieczonka, T., Bolch, T., Wei, J., and Liu, S.: Heterogeneous mass loss of glaciers in the  
684 Aksu-Tarim Catchment (Central Tien Shan) revealed by 1976 KH-9 Hexagon and 2009  
685 SPOT-5 stereo imagery, *Remote Sensing of Environment*, 130, 233–244, 2013.

686 Pieczonka, T. and Bolch, T.: Region-wide glacier mass budgets and area changes for the  
687 Central Tien Shan between ~1975 and 1999 using Hexagon KH-9 imagery, *Global Planet.*  
688 *Change*, in press, 2014.

689 Quincey, D. J., L.Copland, Mayer, C., Bishop, M., A.Luckman, and Belo, M: Ice velocity and  
690 climate variations for Baltora Glacier, Pakistan, *Journal of Glaciology*, 55, 1061-1071, 2009.

691 Reyers, M., Pinto, J. G., and Paeth, H.: Statistical–dynamical downscaling of present day and  
692 future precipitation regimes in the Aksu River Catchment in Central Asia, *Global and*  
693 *Planetary Change*, 107, 36-49, <http://dx.doi.org/10.1016/j.gloplacha.2013.04.003>, 2013.

694 Rignot, E., Echelmeyer, K., and Krabill, W.: Penetration depth of interferometric synthetic-  
695 aperture radar signals in snow and ice, *Geophysical Research Letters*, 28, 3501-3504,  
696 10.1029/2000gl012484, 2001.

697 Schomacker, A.: What controls dead-ice melting under different climate conditions? A  
698 discussion, *Earth-Science Reviews*, 90, 103-113, 2008.

699 Shen, Y.P., Wang, G.Y., Ding, Y.J., Mao, W.Y., Liu, S.Y., Wang, S.D., Duishen M  
700 Mamatkanov: Changes in Glacier Mass Balance in Watershed of Sary Jaz-Kumarik Rivers of  
701 Tianshan Mountains in 1957—2006 and Their Impact on Water Resources and Trend to End  
702 of the 21st Century, *Journal of Glaciology and Geocryology*, 31, 5, 792-801, 2009[in Chinese  
703 with english abstract].

704 Shi, Y., Shen, Y., Kang, E., Li, D., Ding, Y., Zhang, g., and Hu, R.: Recent and future climate  
705 change in northwest China, *Climatic Change*, DOI 10.1007/s10584-006-9121-7, 2006.

706 Shortridge, A., and Messina, J.: Spatial structure and landscape associations of SRTM error,  
707 *Remote Sensing of Environment*, 115, 1576-1587, <http://dx.doi.org/10.1016/j.rse.2011.02.017>,  
708 2011.

709 Sorg, A., Bolch, T., Stoffel, M., Solomina, O., and Beniston, M.: Climate change impacts on  
710 glaciers and runoff in Tien Shan (Central Asia), *Nature Climate Change*, 2, 725–731,  
711 10.1038/nclimate1592, 2012.

712 Surazakov, A. B., and Aizen, V. B.: Estimating volume change of mountain glaciers using  
713 SRTM and Map-Based Topographic data, *IEEE Transactions on Geoscience and Remote  
714 sensing*, 44, 2991-2994, 2006.

715 Surdyk, S.: Using microwave brightness temperature to detect short-term surface air  
716 temperature changes in Antarctica: An analytical approach, *Remote Sensing of Environment*,  
717 80, 256-271, [http://dx.doi.org/10.1016/S0034-4257\(01\)00308-X](http://dx.doi.org/10.1016/S0034-4257(01)00308-X), 2002.

718 Takaku, J., Futamura, N., Iijima, T., Tadono, T., Shimada, M., and Shibasaki, R.: High  
719 resolution DEM generation from ALOS PRISM data - simulation and evaluation, *Geoscience  
720 and Remote Sensing Symposium, 2004. IGARSS '04. Proceedings. 2004 IEEE International,  
721 2004*, 4548-4551 vol.4547.

722 Toutin, T.: Generation of DSMs from SPOT-5 in-track HRS and across-track HRG stereo  
723 data using spatiotriangulation and autocalibration, *Isprs Journal of Photogrammetry and  
724 Remote Sensing*, 60, 170-181, <http://dx.doi.org/10.1016/j.isprsjprs.2006.02.003>, 2006.

725 Uchiyama, Y., Honda, M., Mizuta, Y., Otsuka, K., Ishizeki, T., Okatani, T., and Tamura, E.:  
726 Revising 1:25,000-Scale topographic maps using ALOS/PRISM Imagery, *Bulletin of the  
727 Geographical Survey Institute*, 56, 1-15, 2008.



728 Unger-Shayesteh, K., Vorogushyn, S., Farinotti, D., Gafurov, A., Duethmann, D., Mandychhev,  
729 A., and Merz, B.: What do we know about past changes in the water cycle of Central Asian  
730 headwaters? A review, *Global and Planetary Change*, 110, Part A, 4-25,  
731 <http://dx.doi.org/10.1016/j.gloplacha.2013.02.004>, 2013.

732 USGS: Shuttle Radar Topography Mission, 3 Arc Second scene, Unfilled finished, Global  
733 Land Cover Facility, University of Maryland, College Park, Maryland, February 2000, 2006.

734 Wang, W., Li, Z., Zhang, G., and Li, X.: The processes and characteristics of mass balance on  
735 the Urumqi Glacier No.1 during 1958-2009, *Sciences in Cold and Arid Regions*, 4, 0505-  
736 0513, 10.3724/SP.J.1226.2012.00505, 2012.

737 WGMS: Fluctuations of Glaciers Database. World Glacier Monitoring Service, Zurich,  
738 Switzerland. DOI:10.5904/wgms-fog-2013-11, 2013.

739 Xu, J., Liu, S., Zhang, S., Guo, W., and Wang, J.: Recent Changes in Glacial Area and  
740 Volume on Tuanjiefeng Peak Region of Qilian Mountains, China, *PLoS ONE*, 8, e70574,  
741 10.1371/journal.pone.0070574, 2013.

742 Yang, L., Meng, X., and Zhang, X.: SRTM DEM and its application advances, *International*  
743 *Journal of Remote Sensing*, 32, 3875-3896, 10.1080/01431161003786016, 2011.

744 Zemp, M., Thibert, E., Huss, M., Stumm, D., Rolstad Denby, C., Nuth, C., Nussbaumer, S. U.,  
745 Moholdt, G., Mercer, A., Mayer, C., Joerg, P. C., Jansson, P., Hynek, B., Fischer, A., Escher-  
746 Vetter, H., Elvehøy, H., and Andreassen, L. M.: Reanalysing glacier mass balance  
747 measurement series, *The Cryosphere*, 7, 1227-1245, 10.5194/tc-7-1227-2013, 2013.

748

749

750

### Figure and Table Captions

751 Figure 1. Location and topography of Southern Inylchek Glacier (SIG) and Northern Inylchek  
752 Glacier (NIG). TS is Tian Shan Staion; K is Koilu Staion.

753 Figure 2. Changes in glacier front position of SIG and NIG between ~1975 and 2007. The  
754 background Landsat TM image was acquired in 1990

755 Figure 3. Mean annual flow direction and velocity of SIG in the time intervals 2002 - 2003 (a)  
756 and 2010 - 2011 (b)

757 Figure 4. a: Elevation difference of SIG and NIG between KH-9 (~1975) and SRTM (1999);  
758 b: Elevation difference of SIG and NIG between SRTM (1999) and SPOT-5 (2007); c:  
759 Elevation difference of SIG and NIG between KH-9 (~1975) and SPOT (2007). The altitude  
760 of points a, b, c, d, e, f and g are ~3,080 m a.s.l., ~3,400 m a.s.l., ~3,860 m a.s.l., ~3,430 m  
761 a.s.l., ~3,685 m a.s.l., ~4,000 m a.s.l. and ~4,410 m a.s.l., derived from SRTM. Point a is on  
762 the edge of SPOT DEM and ALOS DEM. From the tongue of SIG to point a, the ice elevation  
763 differences are derived from KH-9 - ALOS in Figure 4b and SRTM - ALOS in Figure 4c.  
764 Point c and point e are on the boundary of KH-9 in 1974 and KH-9 in 1976; Region 2 is in  
765 accumulation of SIG in Figure 4b.

766 Figure 5. Longitudinal profiles of SIG and NIG for the period ~1975 - 1999 (KH-9 - SRTM),  
767 1999 - 2007 (SRTM - SPOT). The section of ALOS PRISM between the tongue of SIG and  
768 point a was derived from SRTM - ALOS in black line.

769 Figure 6. The mean annual elevation difference measured for the period of ~1975 - 1999  
770 (KH-9 - SRTM), 1999 - 2007 (SRTM - SPOT) and ~1975 - 2007 (KH-9 - SPOT) along the  
771 elevation zones in the SIG and NIG. For SIG, the elevation difference in zones 2,800 - 3,000  
772 was derived from KH-9 - ALOS between ~1975 - 2006.

773 Table 1. List of utilized satellite images and data sources

774 Table 2. Uncertainty of glacier delineation (%)

775 Table 3. The SIG and NIG area change between ~1975 and 2007

776 Table 4. Glacier mass changes based on Area-averaged  $dh/dt$  for period ~1975 - 2007

777

778 Table 1. List of utilized satellite images and data sources

| Satellite                          | Time        | Pixel size<br>(nadir,<br>m) | Swatch(Km)           | B/H  | DEM pixel<br>size<br>(m) | Velocity<br>image |   |
|------------------------------------|-------------|-----------------------------|----------------------|------|--------------------------|-------------------|---|
| ALOS                               | Nadir(N)    | Oct., 08,                   | 2.5                  | 35   | 0.5                      | 10                | - |
|                                    | Backward(B) | 2006                        |                      |      |                          |                   |   |
| SPOT-5 HRG                         | Feb., 05,   | 2.5                         | 60                   | 0.63 | 10                       | -                 |   |
|                                    | 2008        |                             |                      |      |                          |                   |   |
| SRTM3 Unfilled<br>Finished version | Feb., 2000  |                             | 1°*1° (tile<br>size) | -    | 90                       | -                 |   |
| SRTM3 filled version               | Feb., 2000  |                             | 1°*1° (tile<br>size) | -    | 90                       | -                 |   |
| Landsat ETM+                       | Oct., 13,   | 15                          | 185                  | -    | -                        | -                 |   |
|                                    | 1999        |                             |                      |      |                          |                   |   |
| Landsat TM                         | Sept., 10,  | 30                          | 185                  | -    | -                        | -                 |   |
|                                    | 1990        |                             |                      |      |                          |                   |   |
| KH-9 Hexagon                       | Nov., 16,   | 6-9                         | 240*120              |      | 25                       | -                 |   |
|                                    | 1974        |                             |                      |      |                          |                   |   |
| KH-9 Hexagon                       | Jan.        | 6-9                         | 240*120              |      | 25                       | -                 |   |
|                                    | 16,1976     |                             |                      |      |                          |                   |   |
| Terra ASTER                        | Aug. 25,    | 15                          | 60                   |      |                          | Yes               |   |
|                                    | 2002        |                             |                      |      |                          |                   |   |
| Terra ASTER                        | Aug. 28,    | 15                          | 60                   |      |                          | Yes               |   |
|                                    | 2003        |                             |                      |      |                          |                   |   |
| Landsat TM                         | Aug. 16,    | 30                          | 185                  |      |                          | Yes               |   |
|                                    | 2010        |                             |                      |      |                          |                   |   |
| Landsat TM                         | Aug. 3,     | 30                          | 185                  |      |                          | Yes               |   |
|                                    | 2011        |                             |                      |      |                          |                   |   |

779

780

781 Table 2. Uncertainty of glacier delineation (%)

|                 | SIG           |      |                 |        | NIG           |      |                 |        |
|-----------------|---------------|------|-----------------|--------|---------------|------|-----------------|--------|
|                 | Landsat<br>TM | KH-9 | Landsat<br>ETM+ | SPOT-5 | Landsat<br>TM | KH-9 | Landsat<br>ETM+ | SPOT-5 |
| Landsat<br>TM   | 2.2           | 2.7  | 2.4             |        | 3.1           | 3.7  | 3.4             |        |
| KH-9            |               | 1.5  | -               | 1.6    |               | 2.1  | -               | 2.1    |
| Landsat<br>ETM+ |               | -    | 1.0             | 1.0    |               | -    | 1.5             | 1.6    |
| SPOT-5          | -             |      | -               | 0.3    | -             |      | -               | 0.6    |

1 Table 3. The SIG and NIG area change between ~1975 and 2007

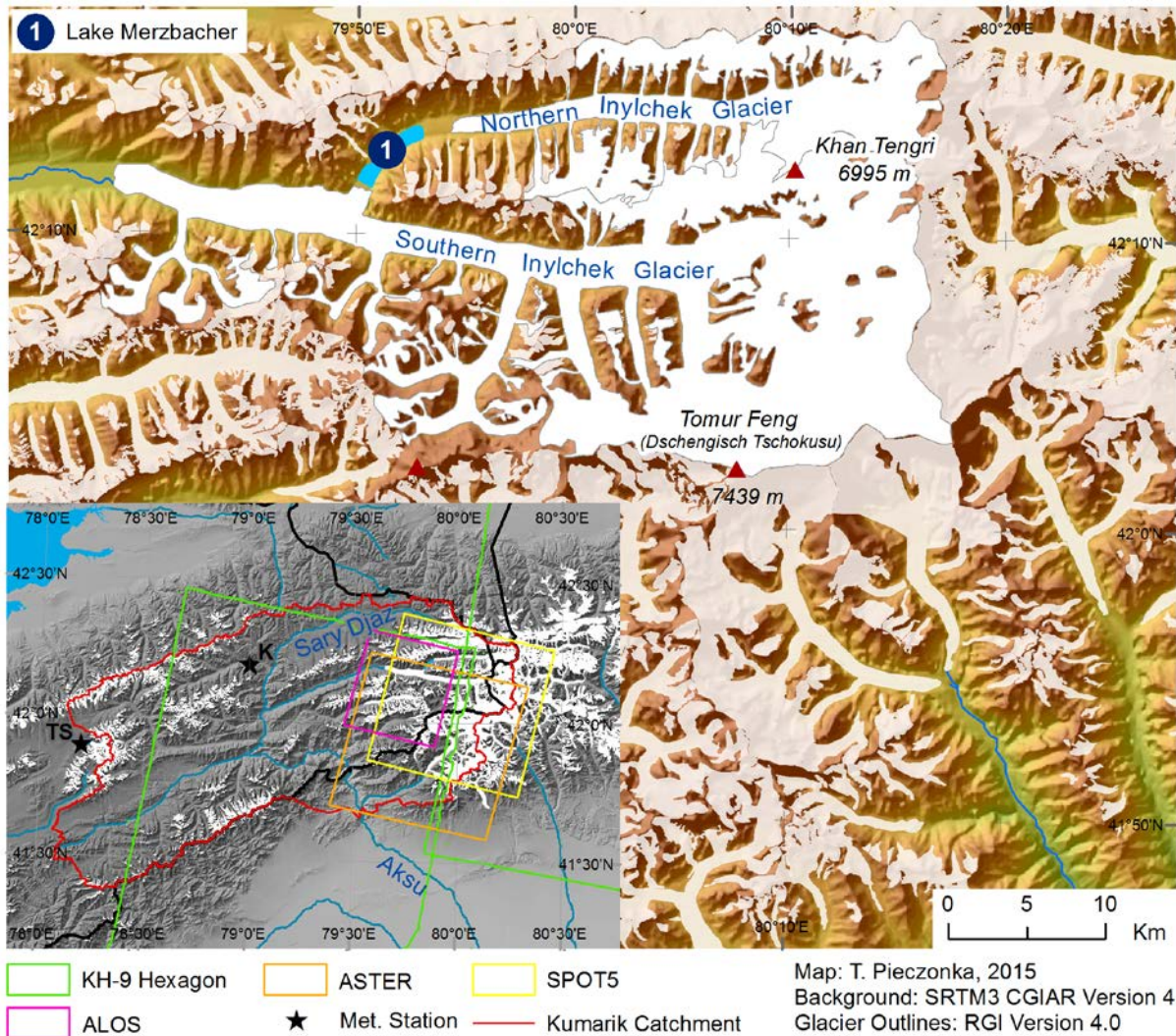
| Year/period  | Area/Area change                                     | SIG            | NIG            |
|--------------|--|----------------|----------------|
| ~1975        | Area (km <sup>2</sup> )                              | 508.4 ± 7.6    | 156.6 ± 3.3    |
| ~1975 - 1990 | Area change (km <sup>2</sup> )                       | -0.1 ± 0.1     | -1.2 ± 0.1     |
|              | Area change (%)                                      | -              | -0.8           |
|              | Annal area change (km <sup>2</sup> a <sup>-1</sup> ) | -0.007 ± 0.007 | -0.08 ± 0.007  |
| 1990 - 1999  | Area change (km <sup>2</sup> )                       | -0.5 ± 0.1     | 3.7 ± 0.1      |
|              | Area change (%)                                      | -0.1           | 2.4            |
|              | Annal area change (km <sup>2</sup> a <sup>-1</sup> ) | -0.056 ± 0.011 | 0.411 ± 0.011  |
| 1999 - 2007  | Area change (km <sup>2</sup> )                       | -0.2 ± 0.1     | -0.4 ± 0.1     |
|              | Area change (%)                                      | -              | -0.3           |
|              | Annal area change (km <sup>2</sup> a <sup>-1</sup> ) | -0.025 ± 0.013 | -0.050 ± 0.013 |
| ~1975 - 2007 | Area change (km <sup>2</sup> )                       | -0.8 ± 0.1     | 2.0 ± 0.1      |
|              | Area change (%)                                      | -0.2           | 1.3            |
|              | Annal area change (km <sup>2</sup> a <sup>-1</sup> ) | -0.025 ± 0.003 | 0.063 ± 0.003  |

1 Table 4. Glacier mass changes based on Area-averaged dh/dt for period ~1975 - 2007

|     |               |                | Altitude zone(m<br>a.s.l.) | Area covered by<br>DEM (km <sup>2</sup> ) | Percentage of total<br>area (%) | Glacier mass changes<br>(m w.e.a <sup>-1</sup> ) |
|-----|---------------|----------------|----------------------------|---|---------------------------------|--|
| SIG | SRTM-<br>KH9  | ~1975-<br>1999 | 2,900-6,600                | 374.5                                     | 73.9                            | -0.43 ± 0.10                                     |
|     | SPOT-<br>SRTM | 1999-<br>2007  | 3,000-6,600                | 241.7                                     | 47.6                            | -0.28 ± 0.46                                     |
|     | SPOT-<br>KH9  | ~1975-<br>2007 | 2,800-6,600                | 388.6                                     | 76.43                           | -0.42 ± 0.11                                     |
| NIG | SRTM-<br>KH9  | ~1975-<br>1999 | 3,300-6,300                | 107.5                                     | 67.6                            | -0.25 ± 0.10                                     |
|     | SPOT-<br>SRTM | 1999-<br>2007  | 3,300-6,400                | 62.7                                      | 39.2                            | -0.57 ± 0.46                                     |
|     | SPOT-<br>KH9  | ~1975-<br>2007 | 3,400-6,600                | 109.9                                     | 69.1                            | -0.30 ± 0.11                                     |

2  
3  
4

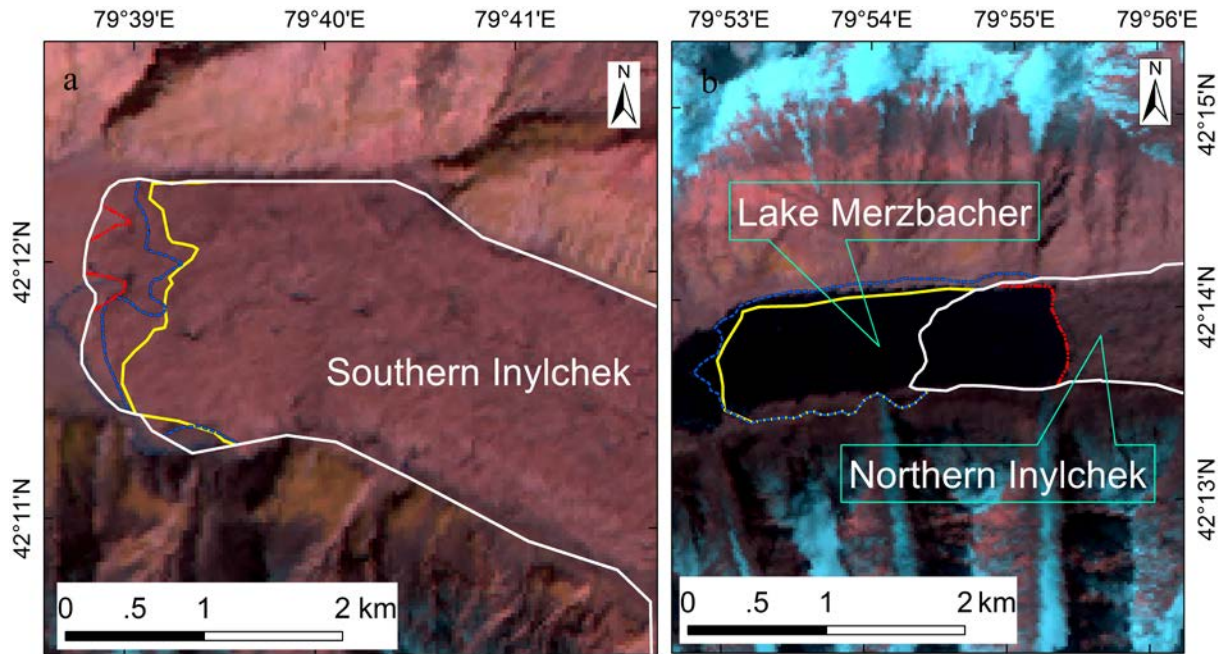
1 Figure 1. Location and topography of Southern Inylchek Glacier (SIG) and Northern Inylchek Glacier  
 2 (NIG). TS is Tian Shan Staion; K is Koilu Staion.



3  
 4  
 5

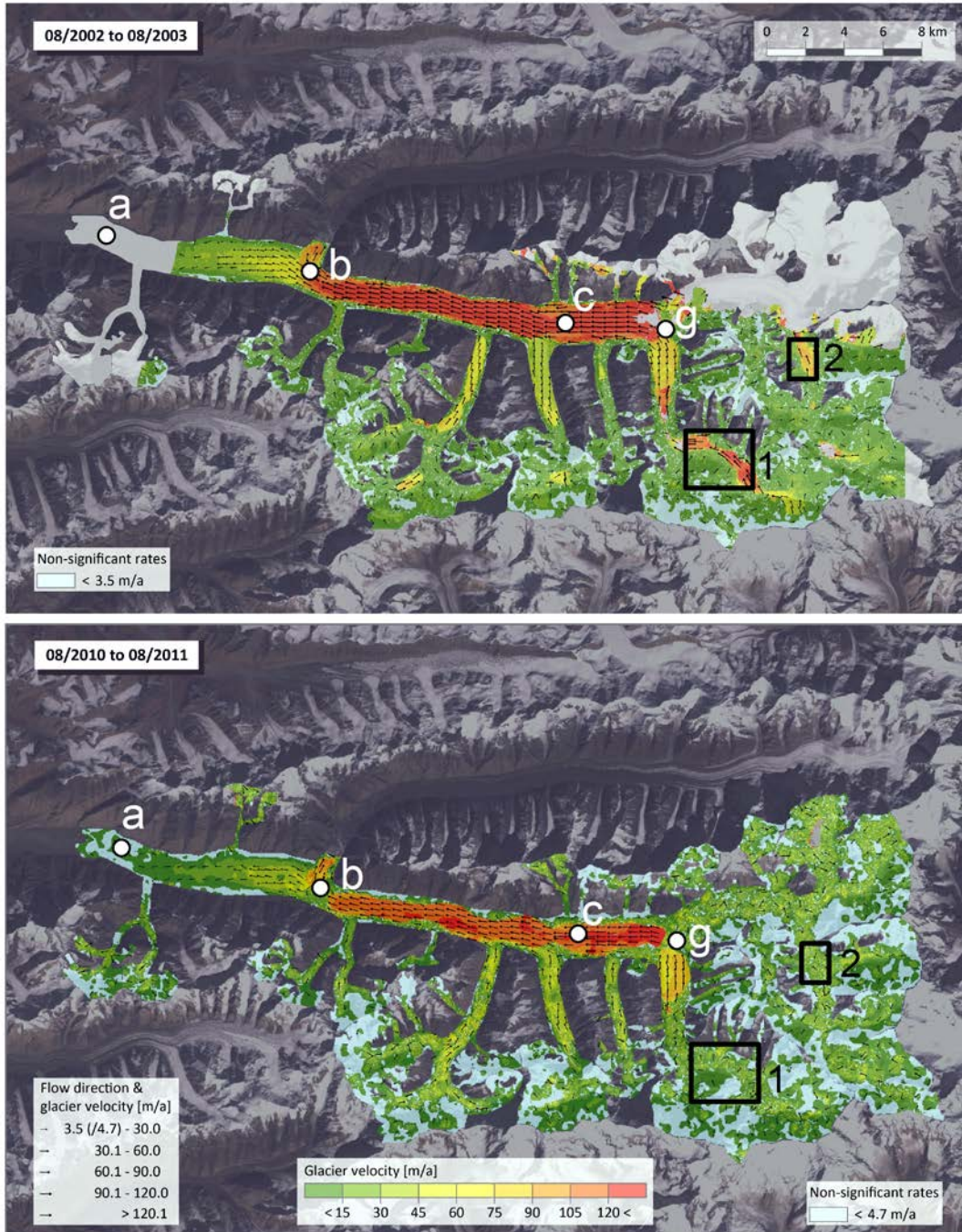


1 Figure 2. Changes in glacier front position of SIG and NIG between ~1975 and 2007. The  
2 background Landsat TM image was acquired in 1990



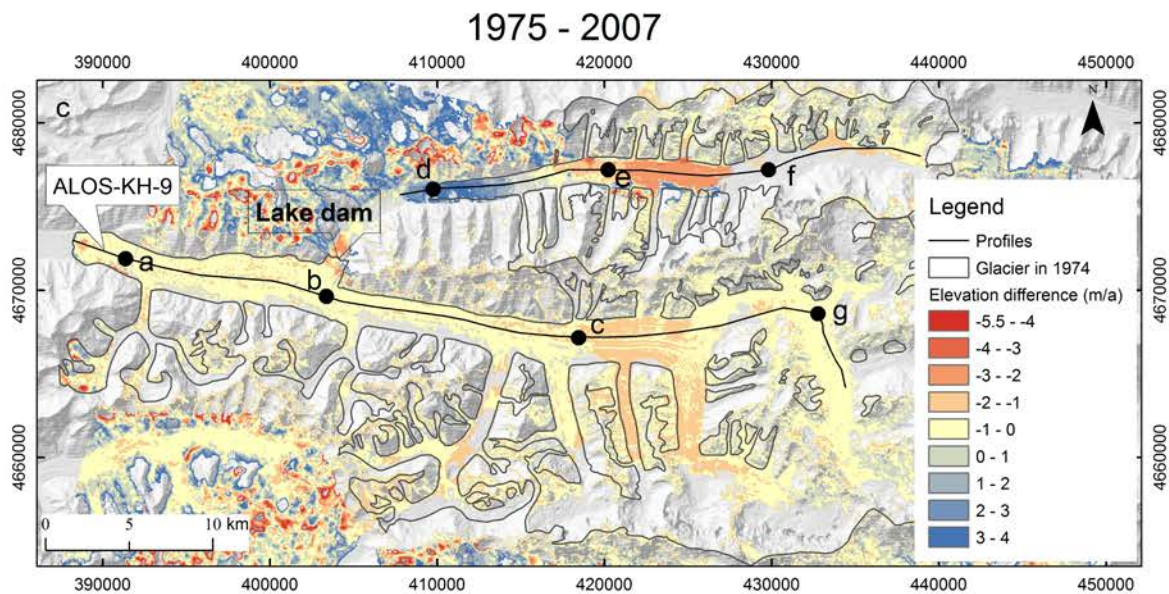
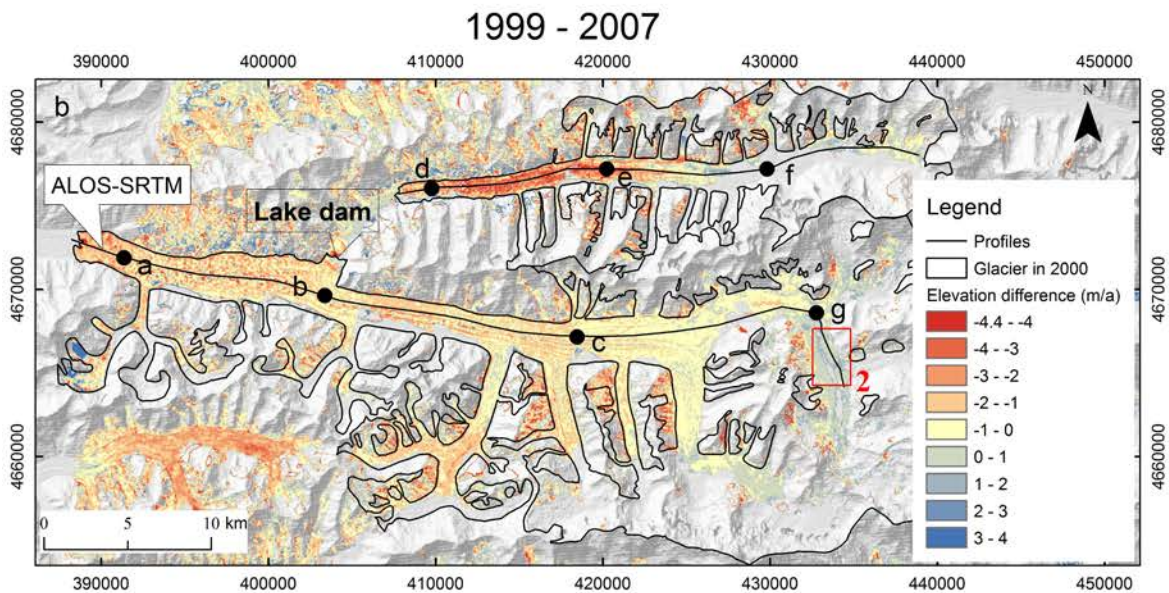
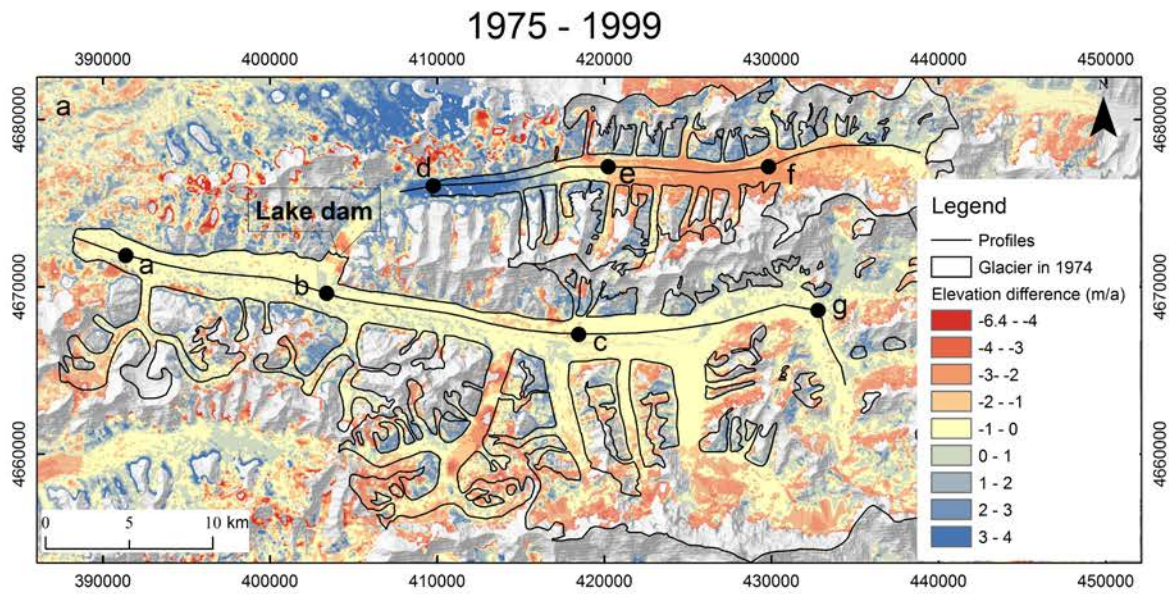
3  
4

1 Figure 3. Mean annual flow direction and velocity of SIG in the time intervals 2002 - 2003 (a)  
 2 and 2010 - 2011 (b)

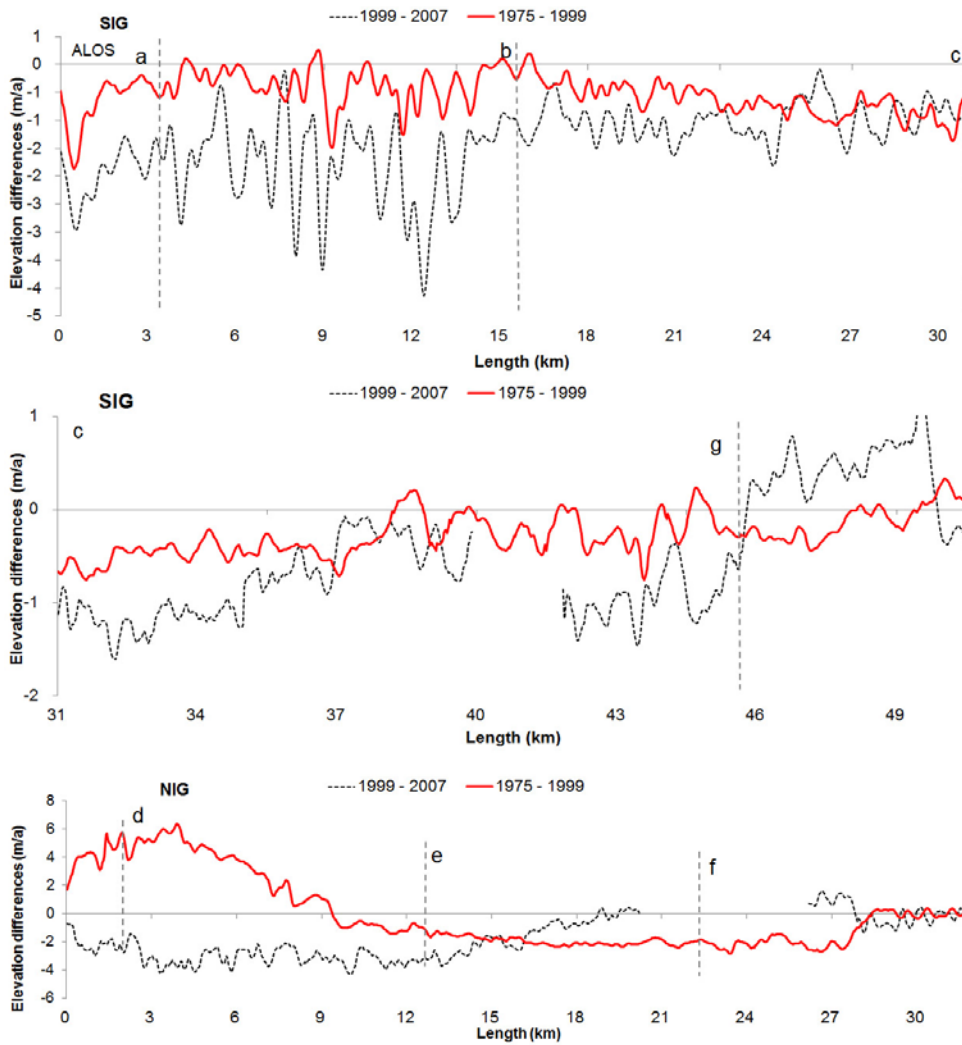


3  
 4

1 Figure 4. a: Elevation difference of SIG and NIG between KH-9 (~1975) and SRTM (1999);  
2 b: Elevation difference of SIG and NIG between SRTM (1999) and SPOT-5 (2007); c:  
3 Elevation difference of SIG and NIG between KH-9 (~1975) and SPOT (2007). The altitude  
4 of points a, b, c, d, e, f and g are ~3,080 m a.s.l., ~3,400 m a.s.l., ~3,860 m a.s.l., ~3,430 m  
5 a.s.l., ~3,685 m a.s.l., ~4,000 m a.s.l. and ~4,410 m a.s.l., derived from SRTM. Point a is on  
6 the edge of SPOT DEM and ALOS DEM. From the tongue of SIG to point a, the ice elevation  
7 differences are derived from KH-9 - ALOS in Figure 4b and SRTM - ALOS in Figure 4c.  
8 Point c and point e are on the boundary of KH-9 in 1974 and KH-9 in 1976; Region 2 is in  
9 accumulation of SIG in Figure 4b.



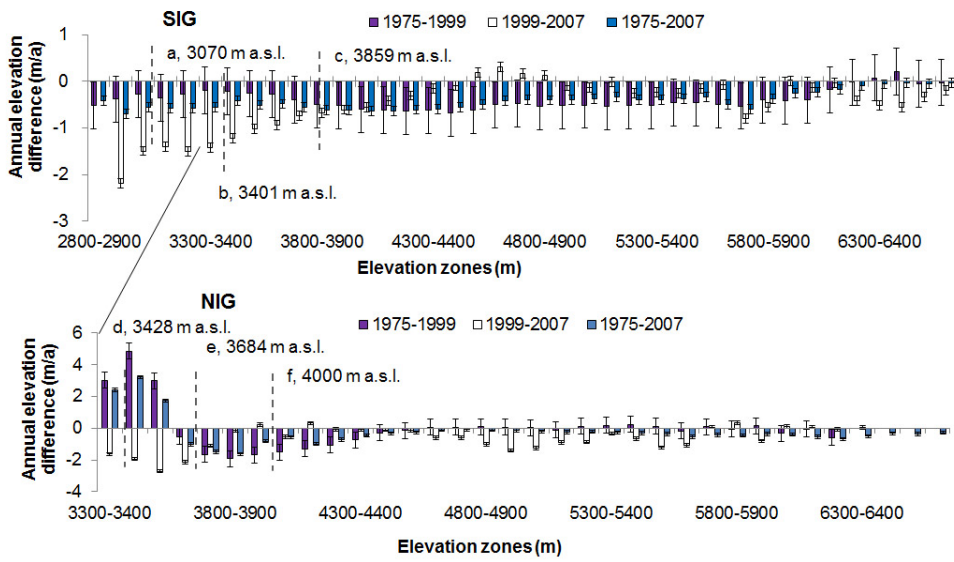
1 Figure 5. Longitudinal profiles of SIG and NIG for the period ~1975 - 1999 (KH-9 - SRTM),  
2 1999 - 2007 (SRTM - SPOT). The section of ALOS PRISM between the tongue of SIG and  
3 point a was derived from SRTM - ALOS in black line.



4

5

1 Figure 6. The mean annual elevation difference measured for the period of ~1975 - 1999  
2 (KH-9 - SRTM), 1999 - 2007 (SRTM - SPOT) and ~1975 - 2007 (KH-9 - SPOT) along the  
3 elevation zones in the SIG and NIG. For SIG, the elevation difference in zones 2,800 - 3,000  
4 was derived from KH-9 - ALOS between ~1975 - 2006



5  
6